Box 15.1 Climate Research: The Pioneers

The French mathematician Jean-Baptiste-Joseph de Fourier (1768-1830) suggested in 1827 that the atmosphere keeps the Earth warm by trapping heat as a plate of glass would. It is known today that the comparison of the atmosphere to a greenhouse is incorrect, but Fourier did suggest that the natural climate could be perturbed as a result of human activities. In 1859, the Irish physicist John Tyndall (1820-1893) measured the absorption of various gases, and established that water vapor, carbon dioxide, and methane were trapping infrared (terrestrial) radiation, while the most abundant atmospheric gases, nitrogen and oxygen, were not. He suggested that ice ages in the past could have been caused by changes in the atmospheric abundance of radiatively active gases.

Tyndall

Arrhenius

In 1896 the Swedish scientist Svante Arrhenius (1859-1927), who was awarded the Nobel Prize for Chemistry in 1903, theorized that a doubling in the natural concentration of carbon dioxide in the air would increase the Earth's global mean temperature by 5-6 degrees Celsius. He pointed out that such a change was likely due to the rapid expansion of industry, and because, as he stated, "we are evaporating our coal mines into the air." In 1938 Guy Stewart Callendar, an engineer working for British Electrical Industries, noted that the level of CO_2 had increased by some 10 percent since the 1890s and that it could explain the rise in temperature recorded over the same period of time.

It was not, however, until the early 1960s that the potential importance of global warming was recognized after the American geochemist Charles D. Keeling reported a continuous increase in the abundance of CO_2 observed in a region as remote as the Mauna Loa Observatory in Hawaii. In the past decades, the question of global warming has led to much debate and even to controversies. The complexity of the problem, including the role played by atmospheric constituents other than CO_2, is taken into account in current studies.

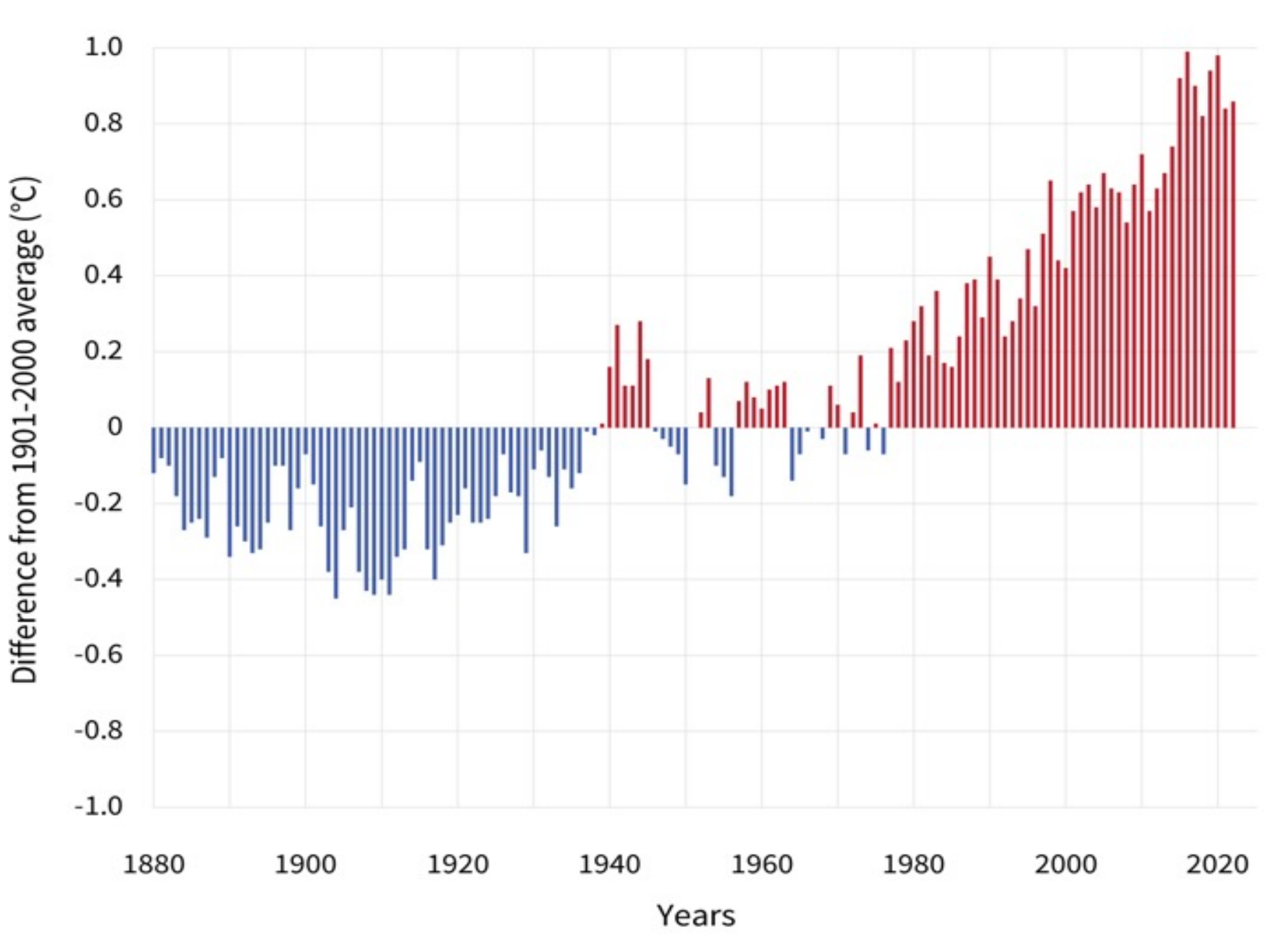
1.0
0.8
0.6
0.4
0.2
0
-0.2
-0.4
-0.6
-0.8
-1.0
Difference from 1901-2000 average (°C)
1880
1900
1920
1940
1960
1980
2000
2020
Years

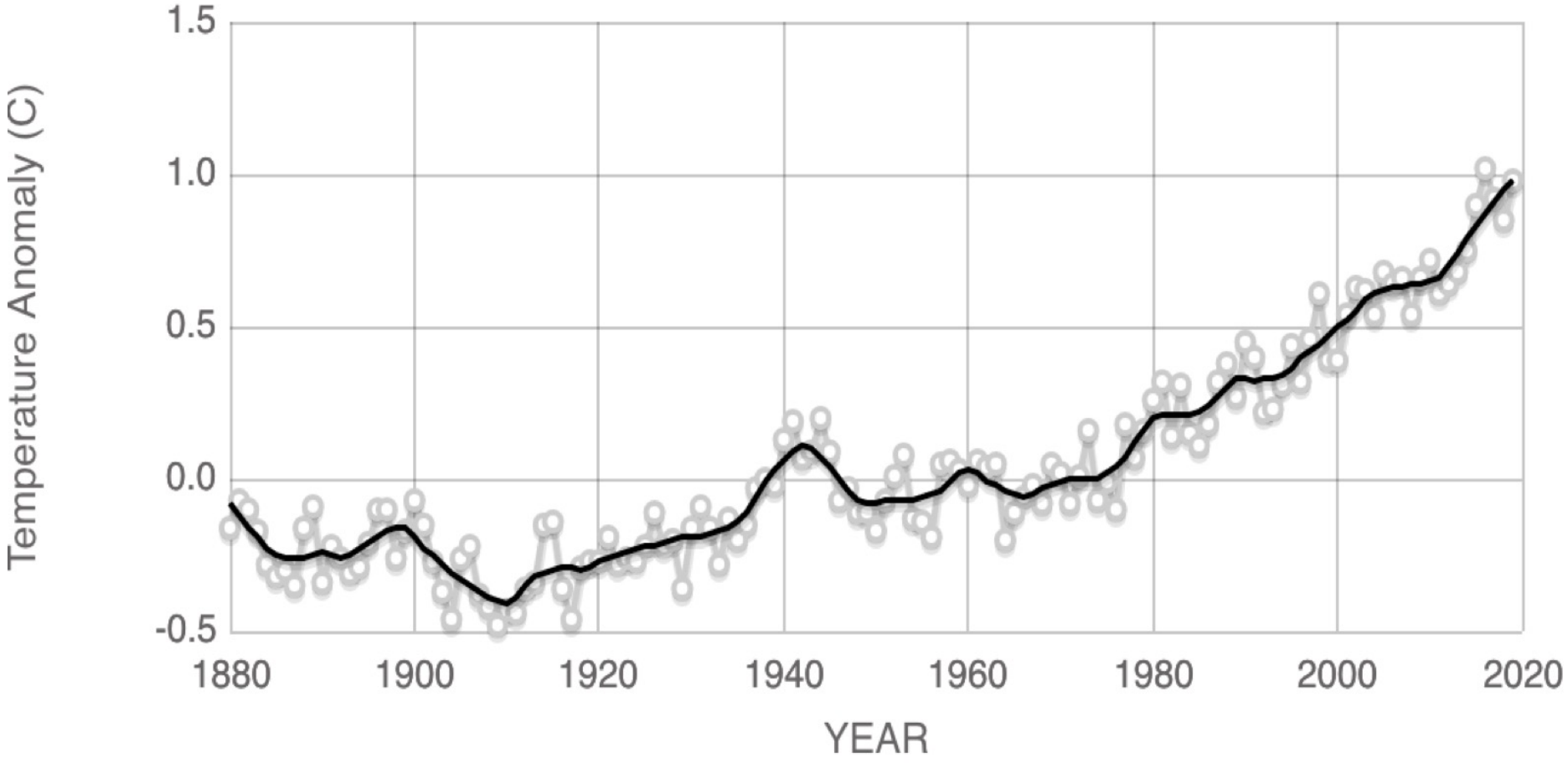

Source: climate.nasa.gov

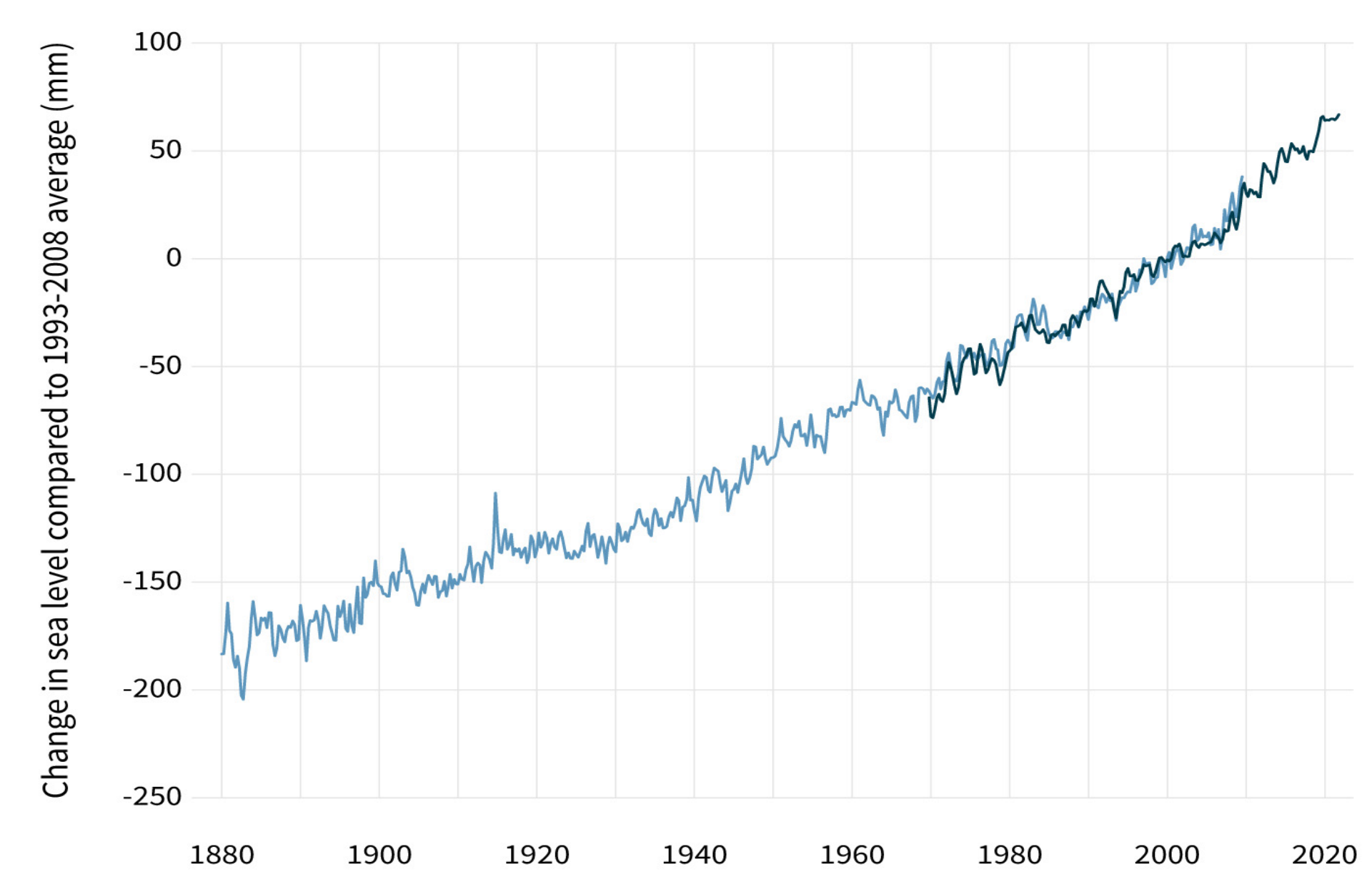

Seasonal (3-month) sea level estimates from Church and White (2011) (light blue line) and University of Hawaii Fast Delivery sea level data (dark blue). The values are shown as change in sea level in millimeters compared to the 1993-2008 average. NOAA Climate.gov image based on analysis and data from Philip Thompson, University of Hawaii Sea Level Center.

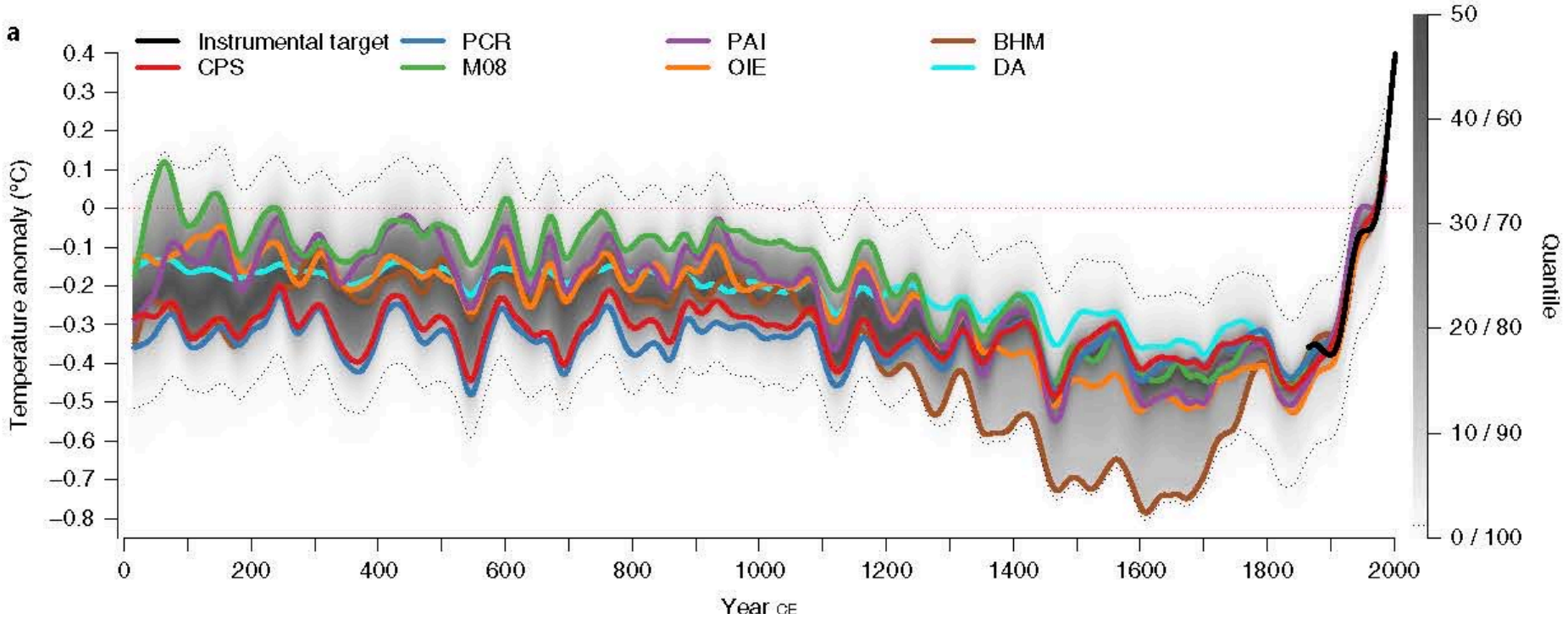

Newcom et al. 2019 NatureGeoscience

Departure of temperature from long term average (°F)
March 2014

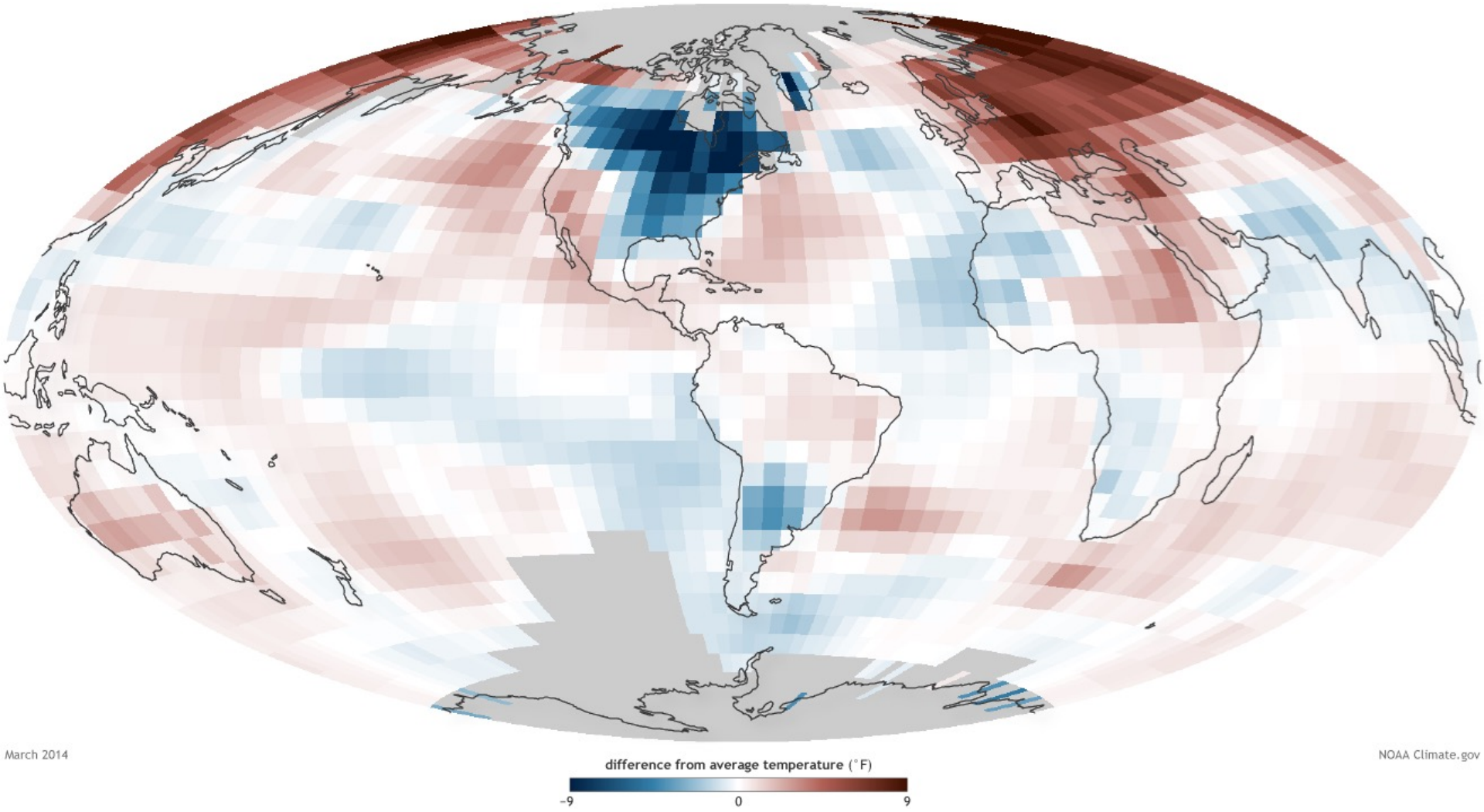

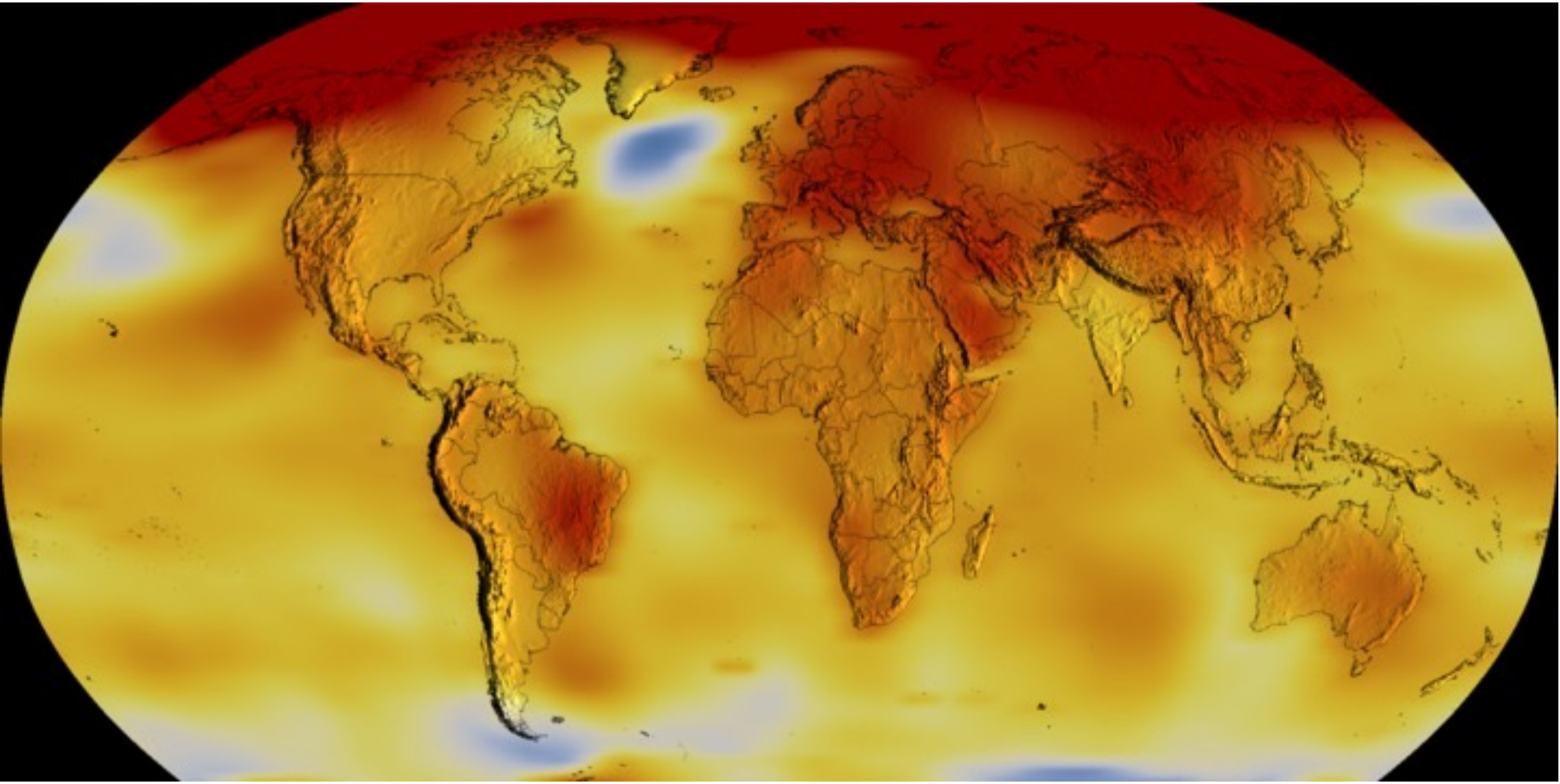

January 2019 departure from 1880, color range -2 to +4F

https://climate.nasa.gov/vital-signs/global-temperature/


February 5 2020 Imperial Palace Kyoto


February 5 2020 Demachiyanagi


February 5 2020 Demachiyanagi


February 9 2020


February 9 2020

February 9 2020

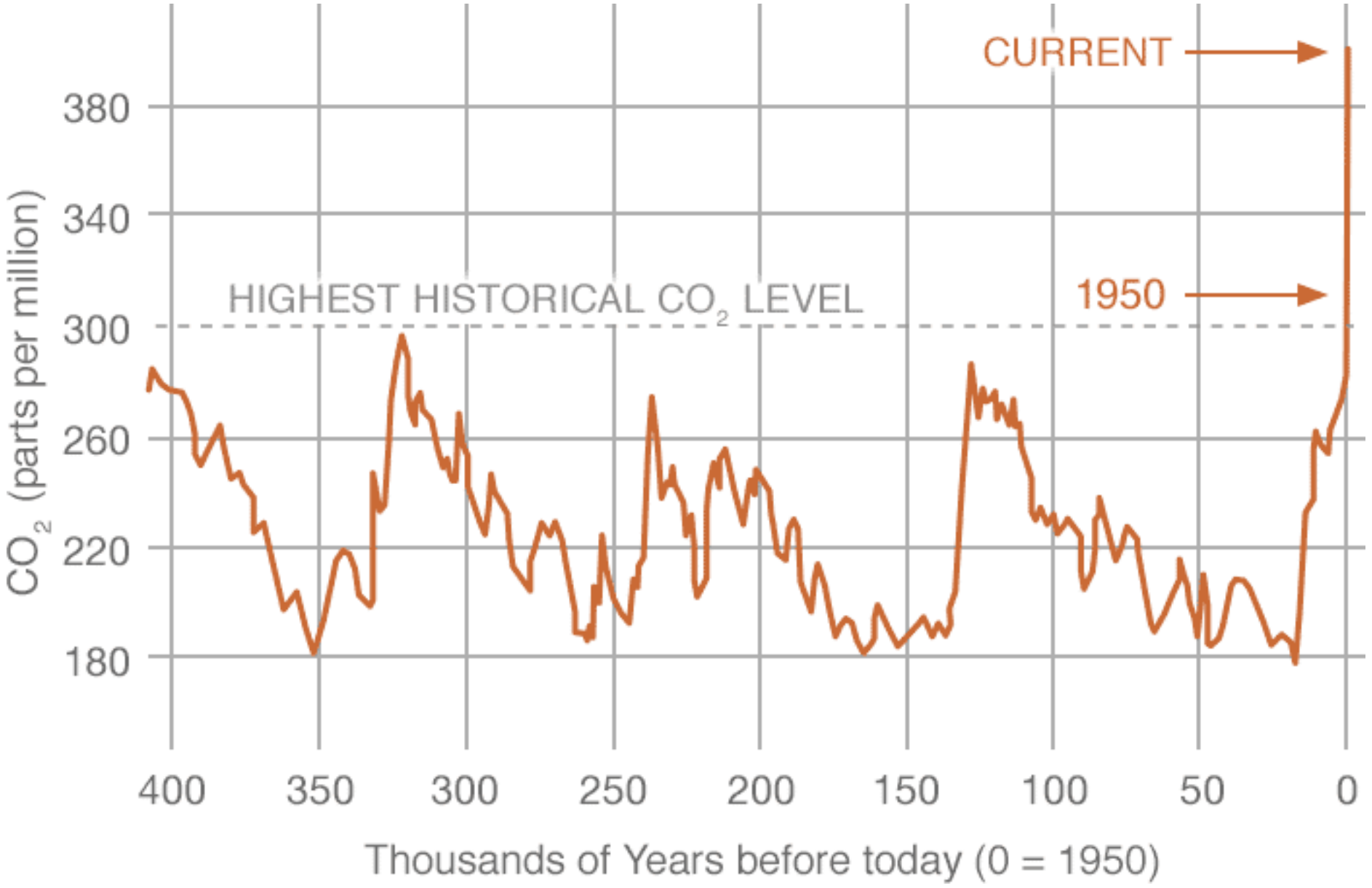
CURRENT
380
340
HIGHEST HISTORICAL CO_2 LEVEL
1950
300
260
220
180
CO_2 (parts per million)
400
350
300
250
200
150
100
50
0
Thousands of Years before today (0 = 1950)


NOAA

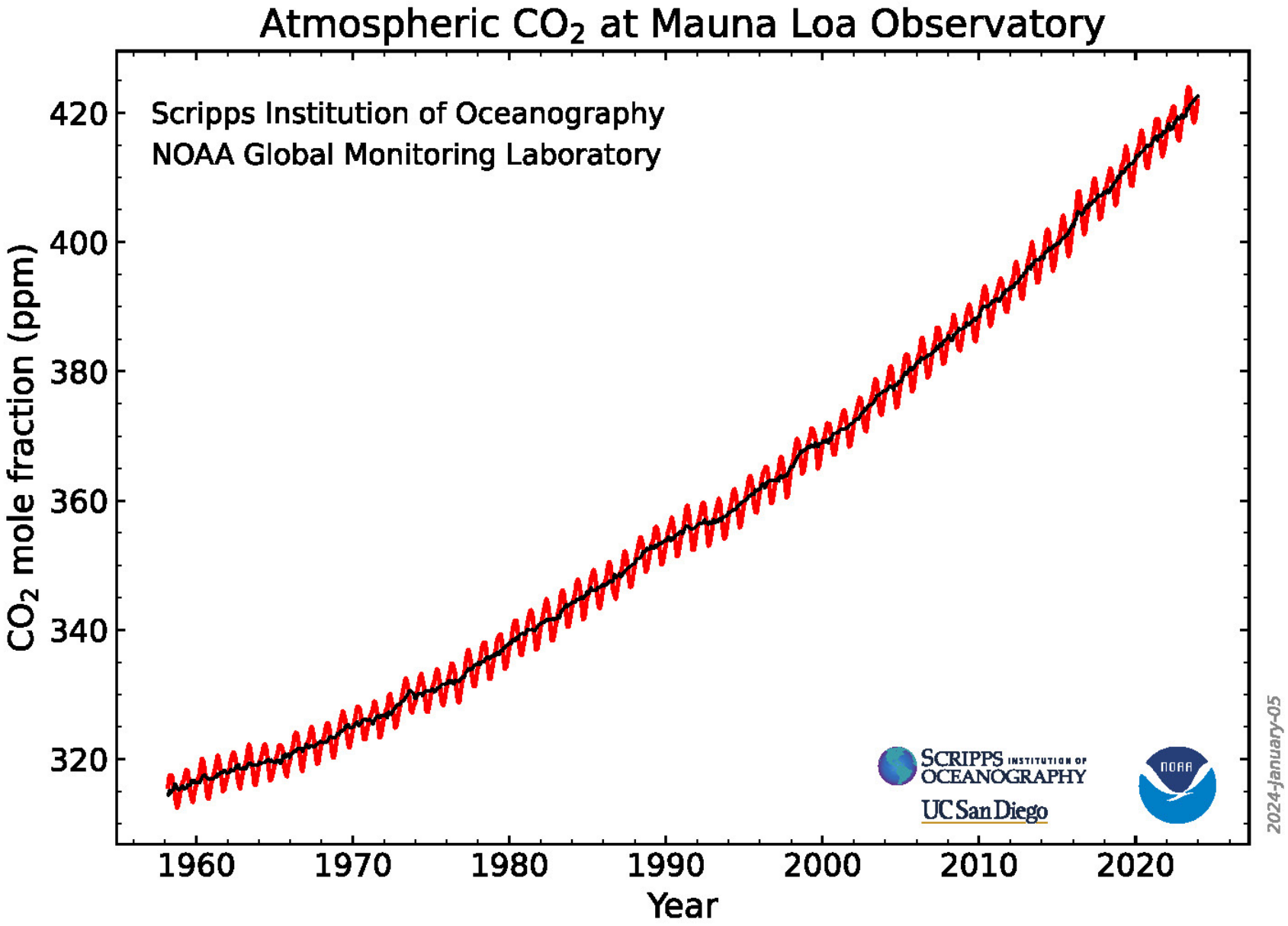
Atmospheric CO_2 at Mauna Loa Observatory
Scripps Institution of Oceanography
NOAA Global Monitoring Laboratory
CO_2 mole fraction (ppm)
420
400
380
360
340
320
1960
1970
1980
1990
2000
2010
2020
Year
SCRIPPS INSTITUTION OF OCEANOGRAPHY
UC San Diego
NOAA
2024-january-05

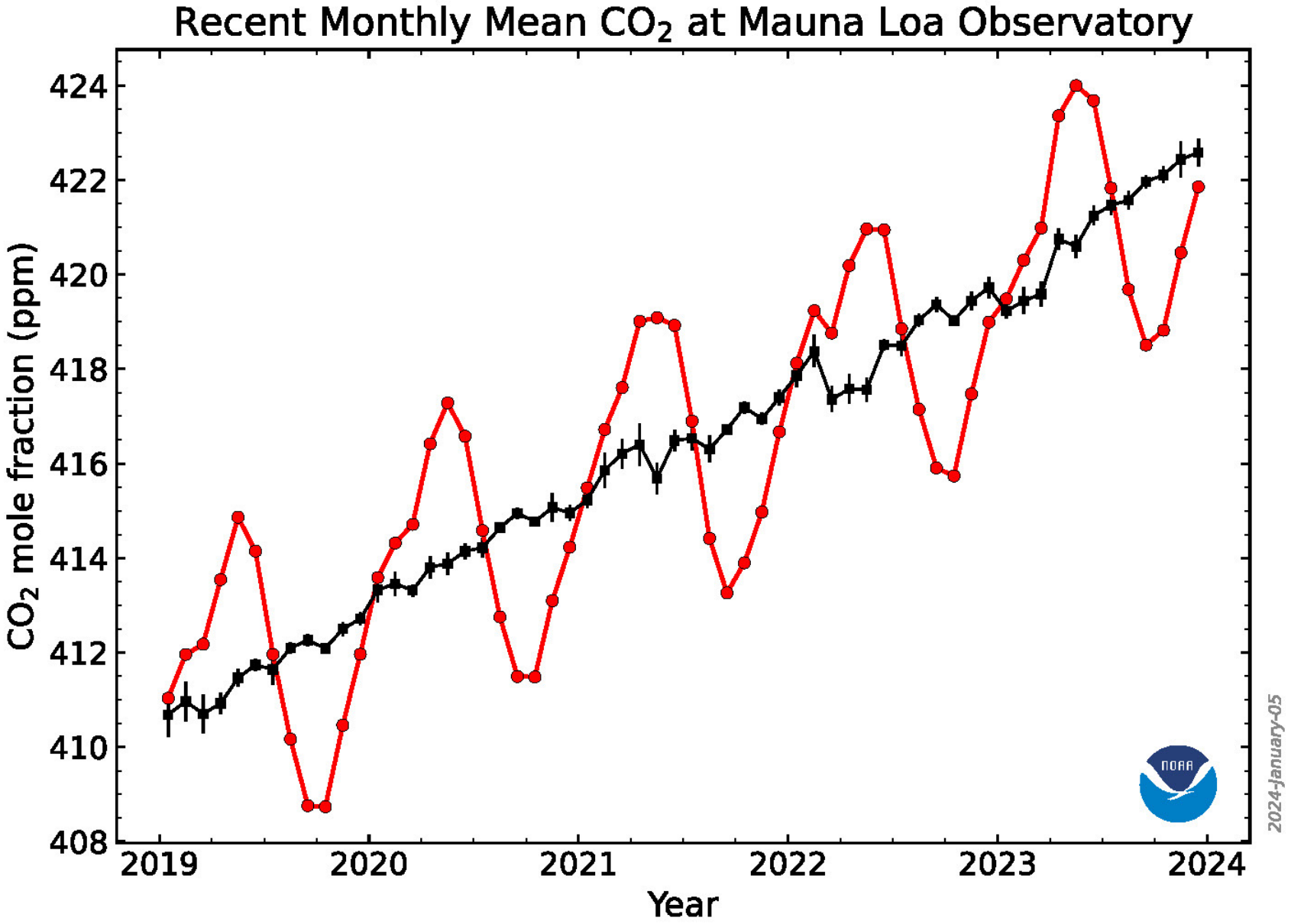
Recent Monthly Mean CO_2 at Mauna Loa Observatory
CO_2 mole fraction (ppm)
424
422
420
418
416
414
412
410
408
2019
2020
2021
2022
2023
2024
Year
NOAA
2024-january-05

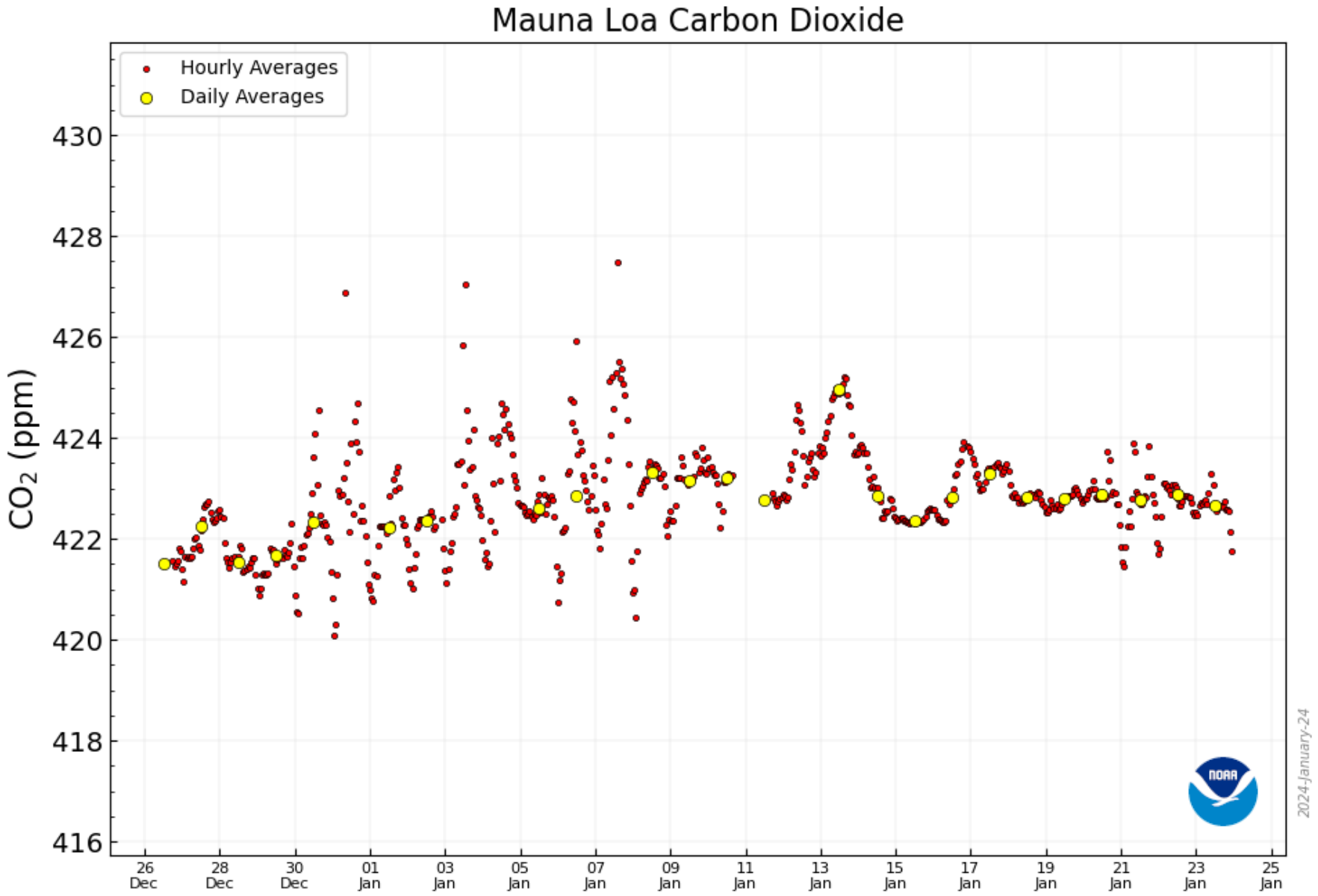
Mauna Loa Carbon Dioxide
Hourly Averages
Daily Averages
CO_2 (ppm)
430
428
426
424
422
420
418
416
26 Dec
28 Dec
30 Dec
01 Jan
03 Jan
05 Jan
07 Jan
09 Jan
11 Jan
13 Jan
15 Jan
17 Jan
19 Jan
21 Jan
23 Jan
25 Jan
NOAA
2024-January-24

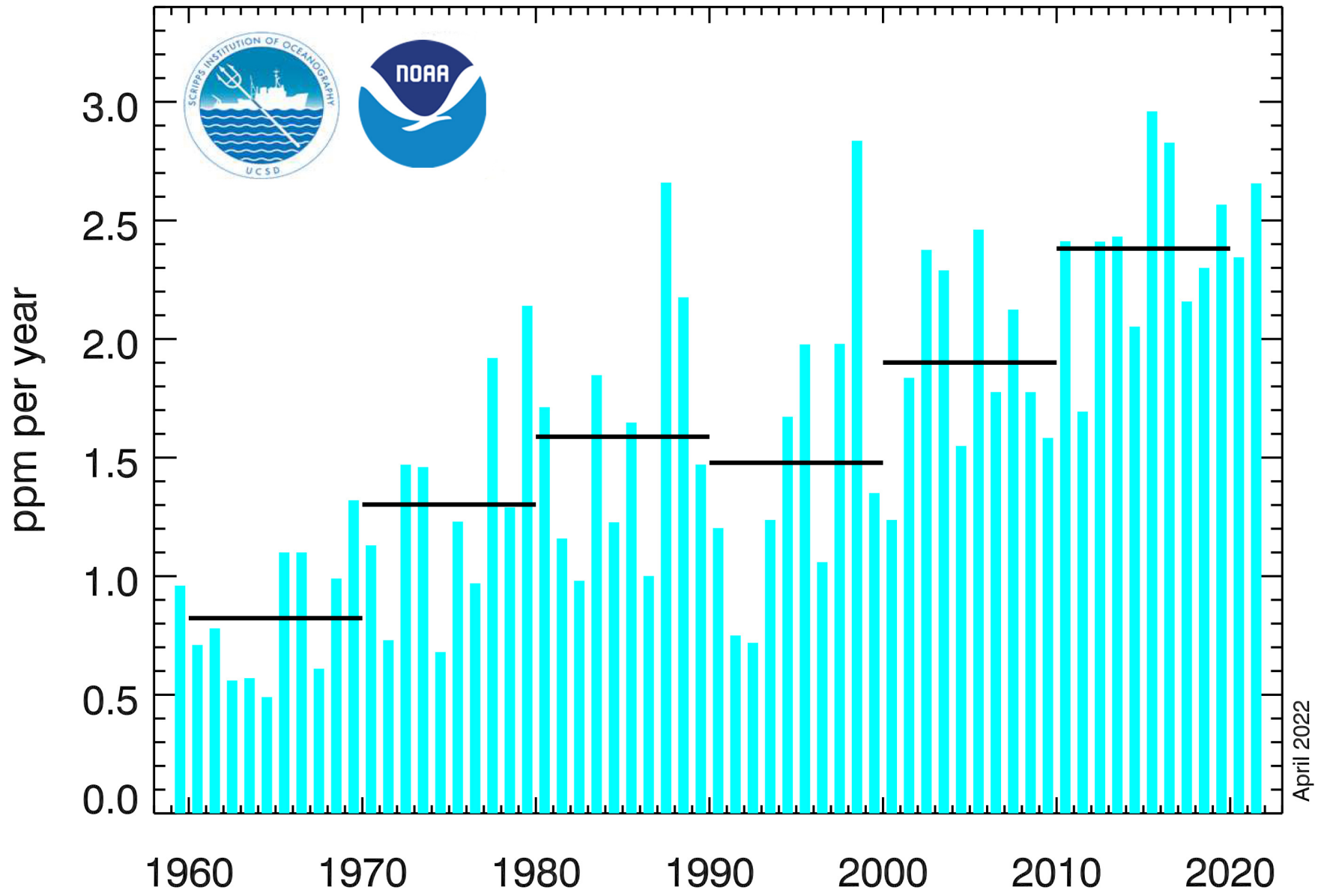
Annual mean global growth rate of CO_2
ppm per year
3.0
2.5
2.0
1.5
1.0
0.5
0.0
1960
1970
1980
1990
2000
2010
2020
April 2022
NOAA
SCRIPPS INSTITUTION OF OCEANOGRAPHY
UCSD

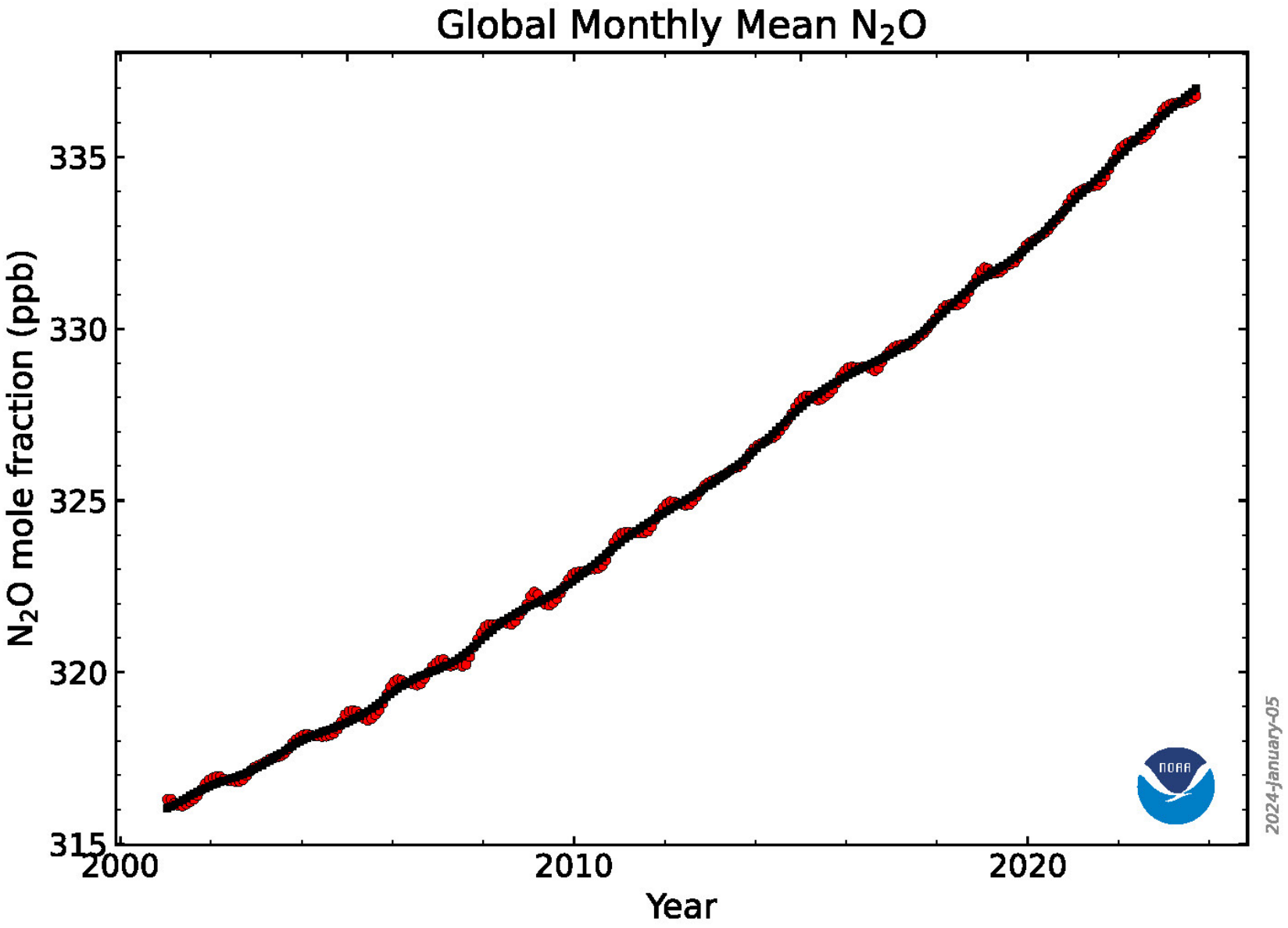
Global Monthly Mean N_2O
N_2O mole fraction (ppb)
315
320
325
330
335
2000
2010
2020
Year
NOAA
2024-January-05

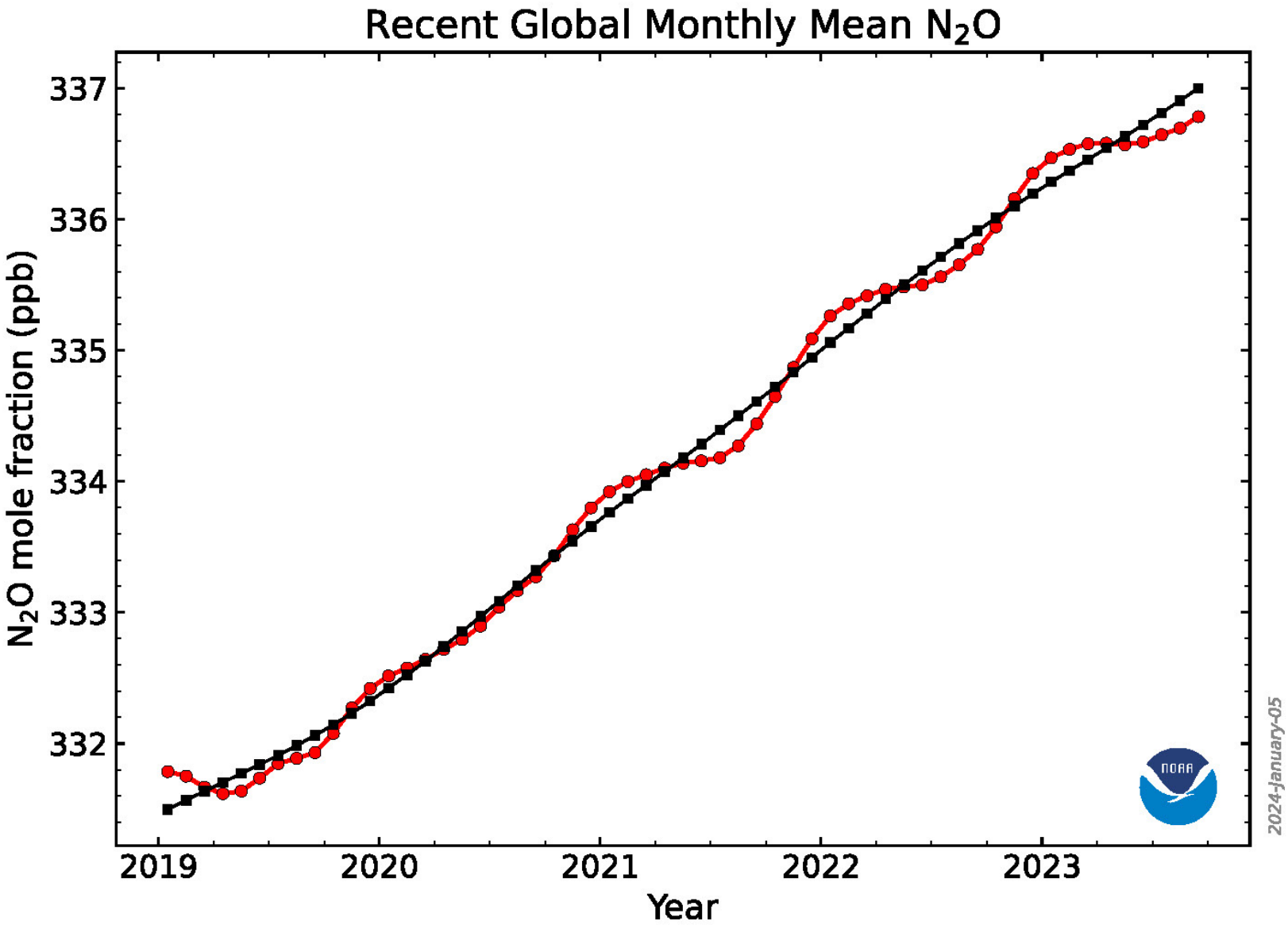
Recent Global Monthly Mean N_2O
N_2O mole fraction (ppb)
337
336
335
334
333
332
2019
2020
2021
2022
2023
Year
NOAA
2024-January-05

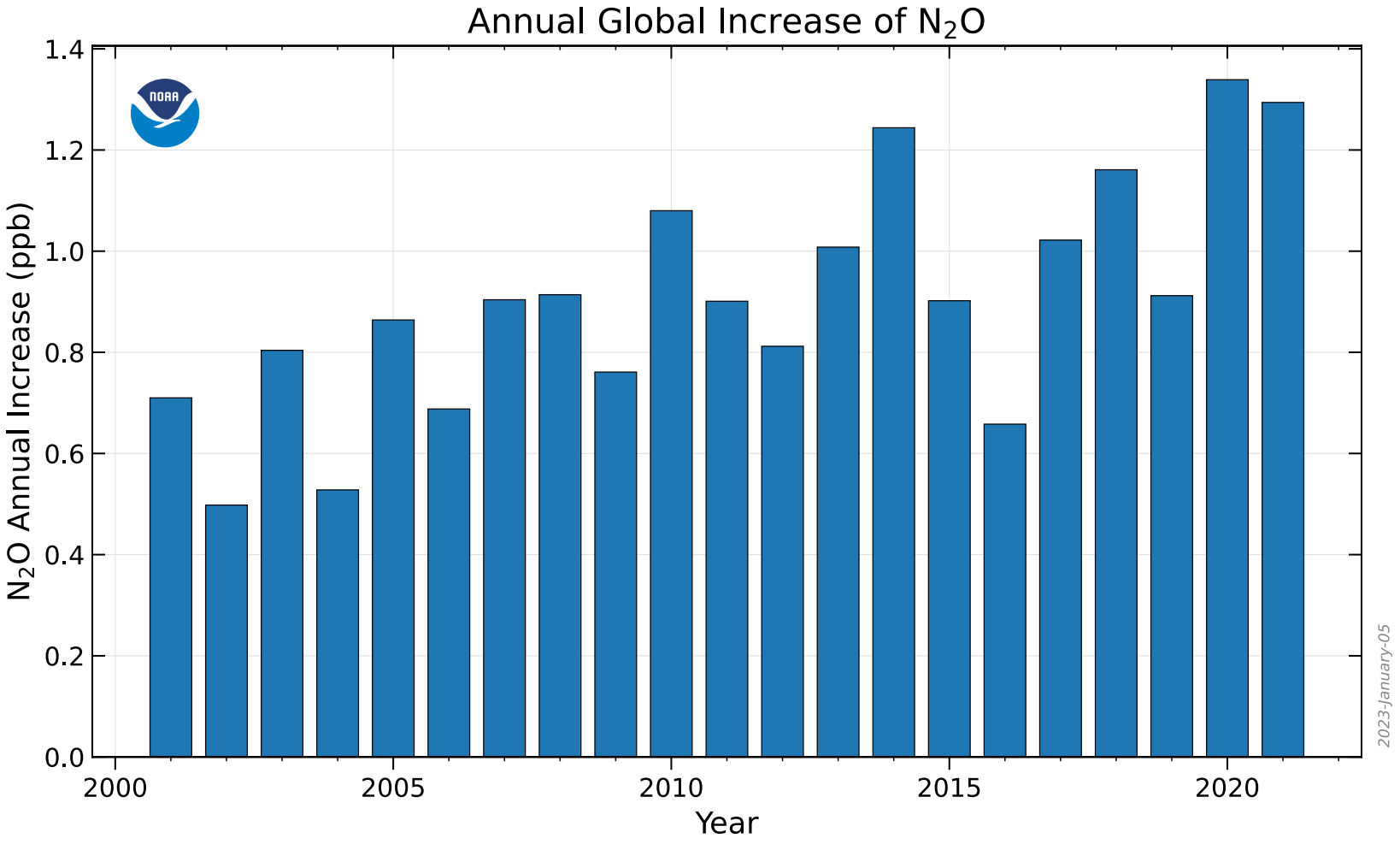
Annual Global Increase of N_2O
N_2O Annual Increase (ppb)
1.4
1.2
1.0
0.8
0.6
0.4
0.2
0.0
2000
2005
2010
2015
2020
Year
2023-January-05

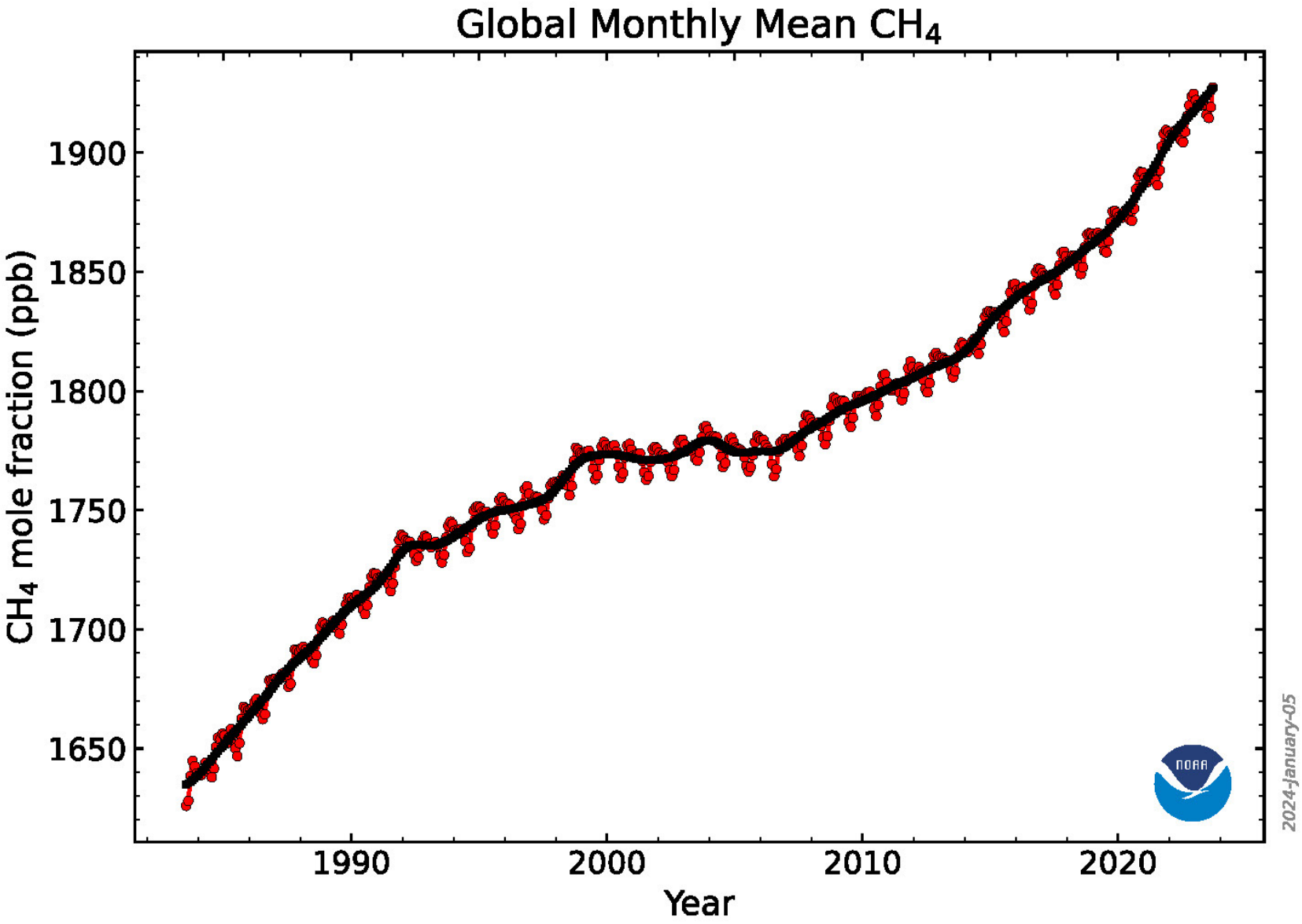
Global Monthly Mean CH_4
CH_4 mole fraction (ppb)
1900
1850
1800
1750
1700
1650
1990
2000
2010
2020
Year
NOAA
2024-January-05

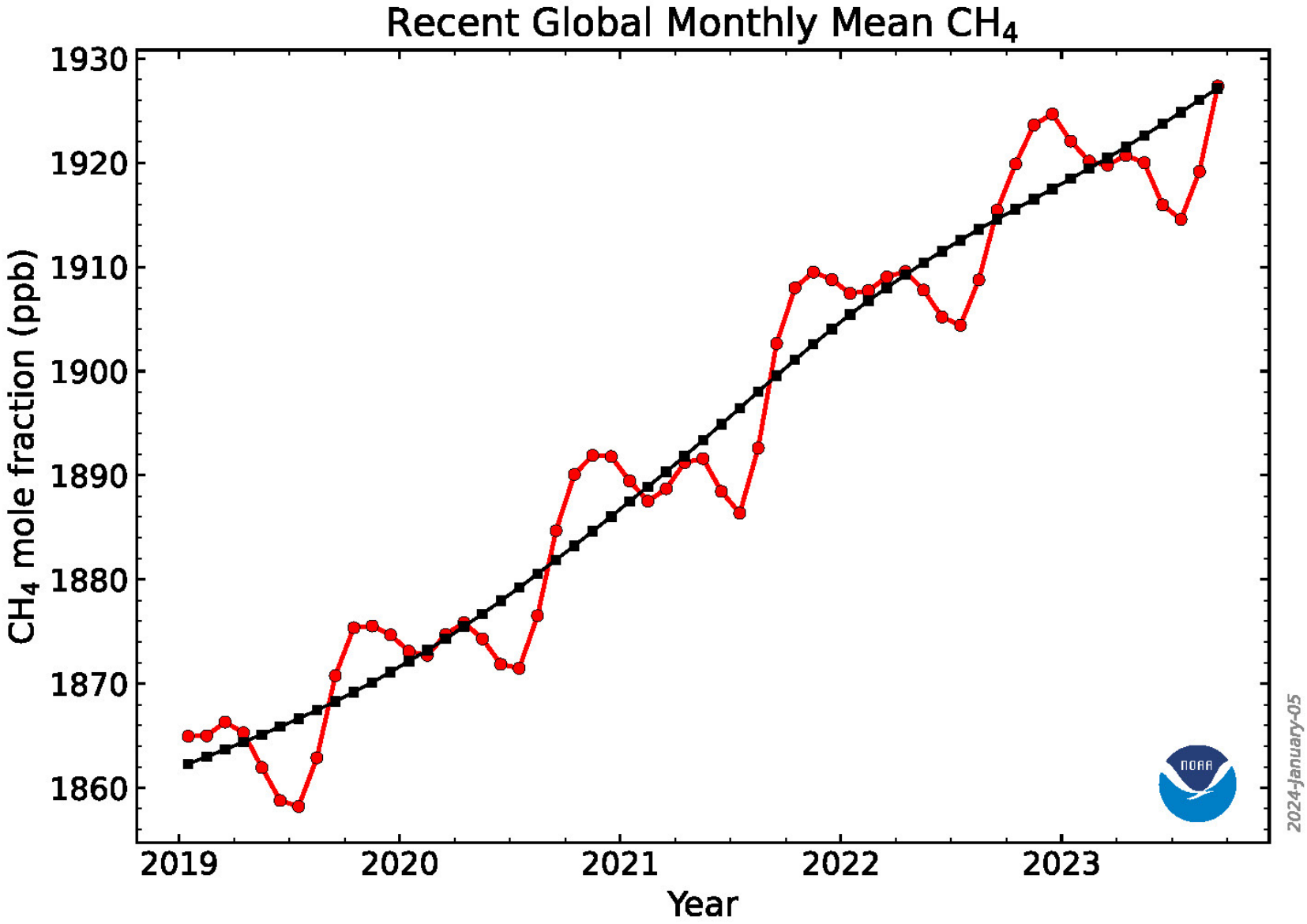
Recent Global Monthly Mean CH_4
CH_4 mole fraction (ppb)
1930
1920
1910
1900
1890
1880
1870
1860
2019
2020
2021
2022
2023
Year
NOAA
2024-january-05

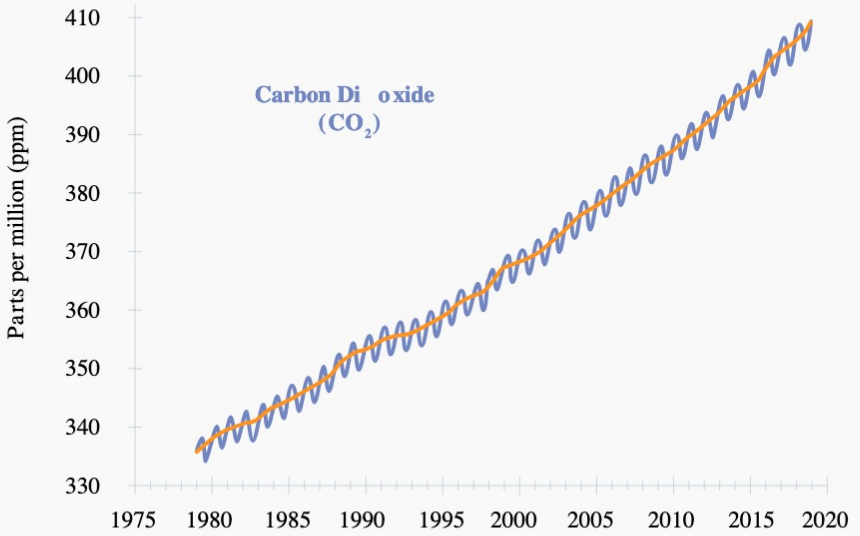
Carbon Di oxide
(CO_2)
Parts per million (ppm)
410
400
390
380
370
360
350
340
330
1975
1980
1985
1990
1995
2000
2005
2010
2015
2020

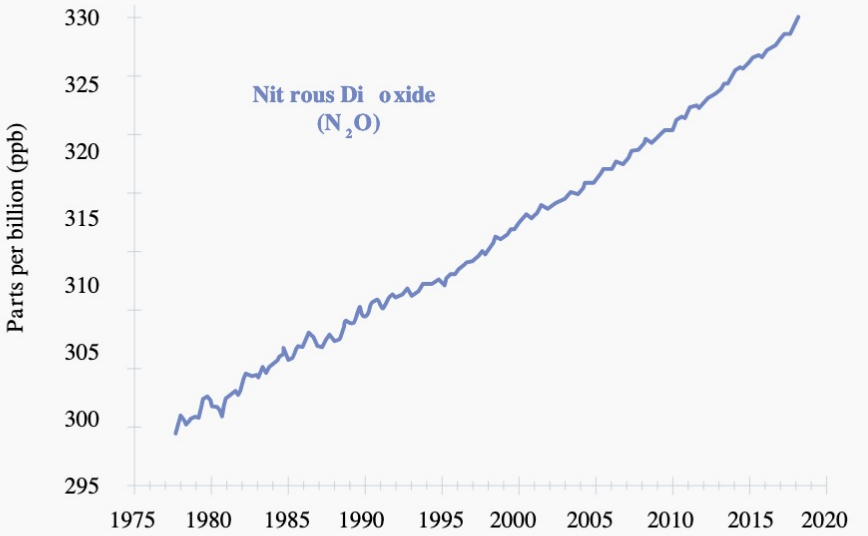
Nit rous Di oxide
(N_2O)
Parts per billion (ppb)
330
325
320
315
310
305
300
295
1975
1980
1985
1990
1995
2000
2005
2010
2015
2020

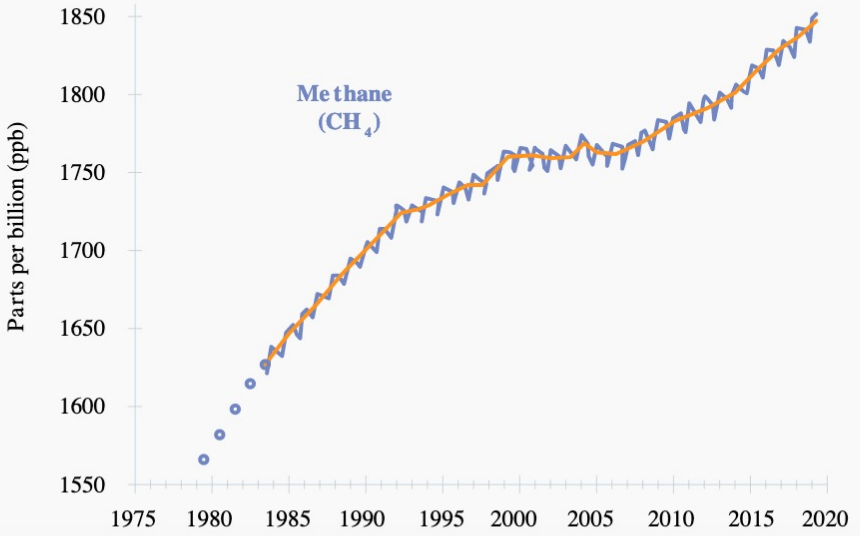
Methane
(CH_4)
Parts per billion (ppb)
1850
1800
1750
1700
1650
1600
1550
1975
1980
1985
1990
1995
2000
2005
2010
2015
2020

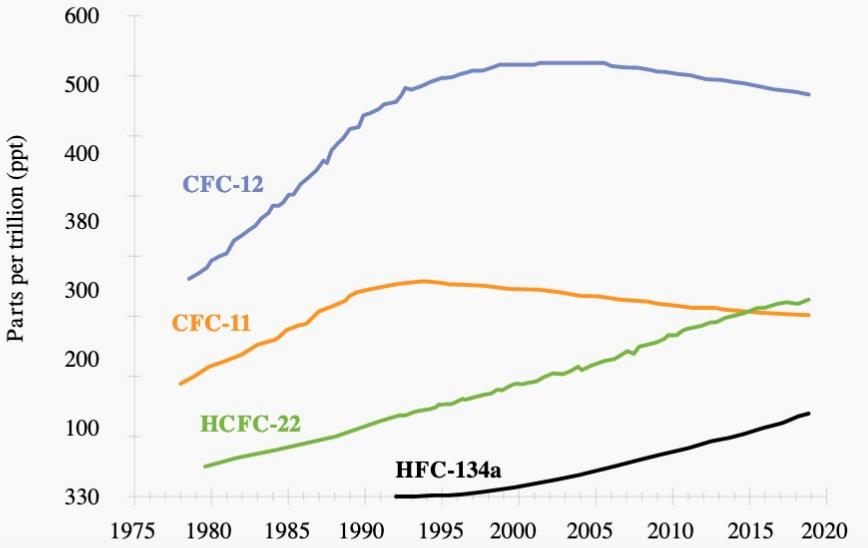
CFC-12
CFC-11
HCFC-22
HFC-134a
Parts per trillion (ppt)
600
500
400
380
300
200
100
330
1975
1980
1985
1990
1995
2000
2005
2010
2015
2020

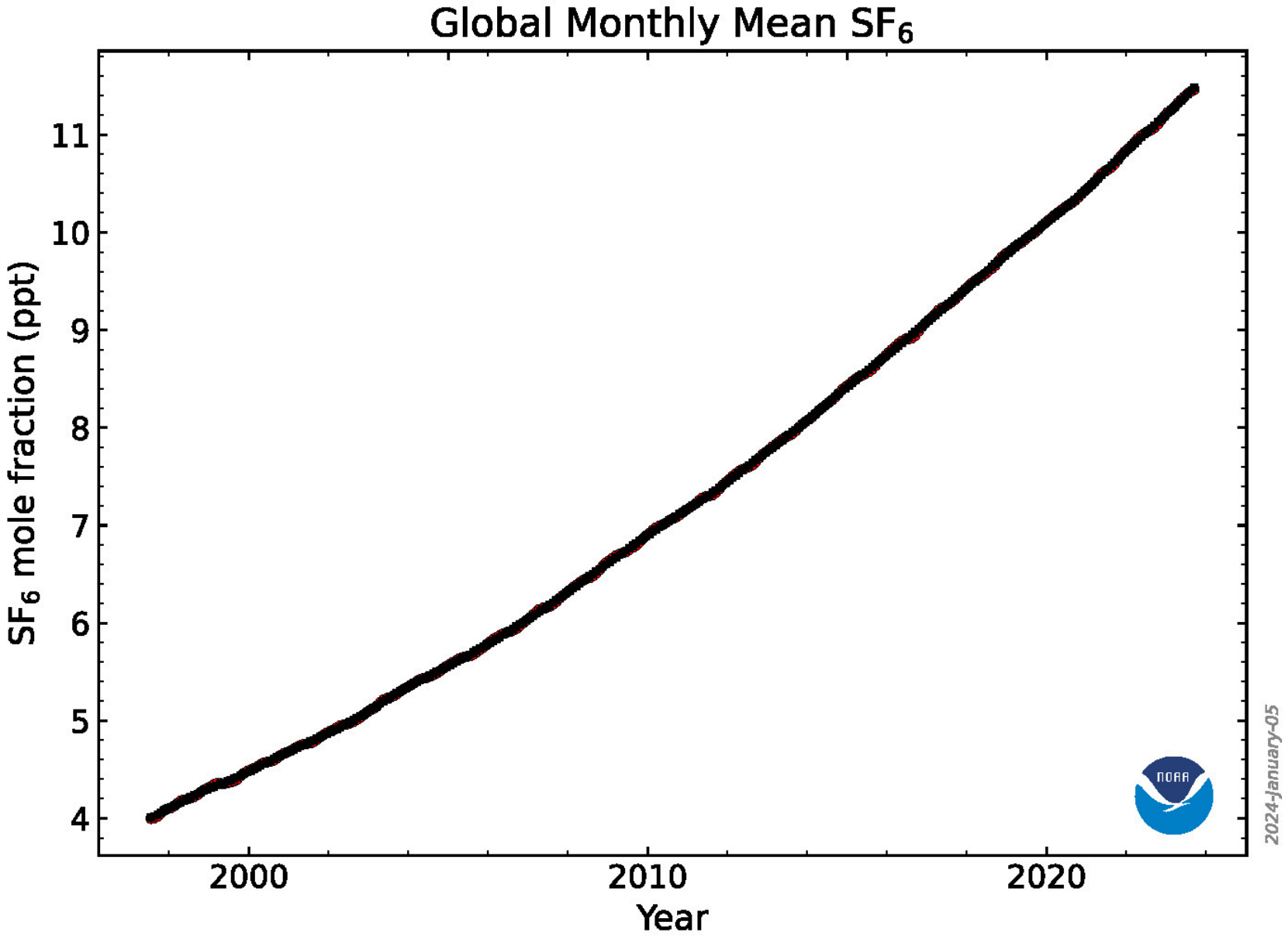
Global Monthly Mean SF_6
SF_6 mole fraction (ppt)
11
10
9
8
7
6
5
4
2000
2010
2020
Year
NOAA
2024-January-05

SF_6 "Sulfur hexafluoride"

- The lifetime of SF_6 in the atmosphere is ~ 580 years - 3,200 years.
- It is primarily used in electrical circuit breakers and high-voltage gas-insulated switchgear.
- On average, one SF_6 gas molecule traps 25,000 times more heat in the atmosphere than one CO_2 molecule, over a century-long time scale.
- Its emissions are likely to influence the Earth's climate for thousands of years.
- Luckily, it is still in the parts per trillion category (parts per 10^{12}).

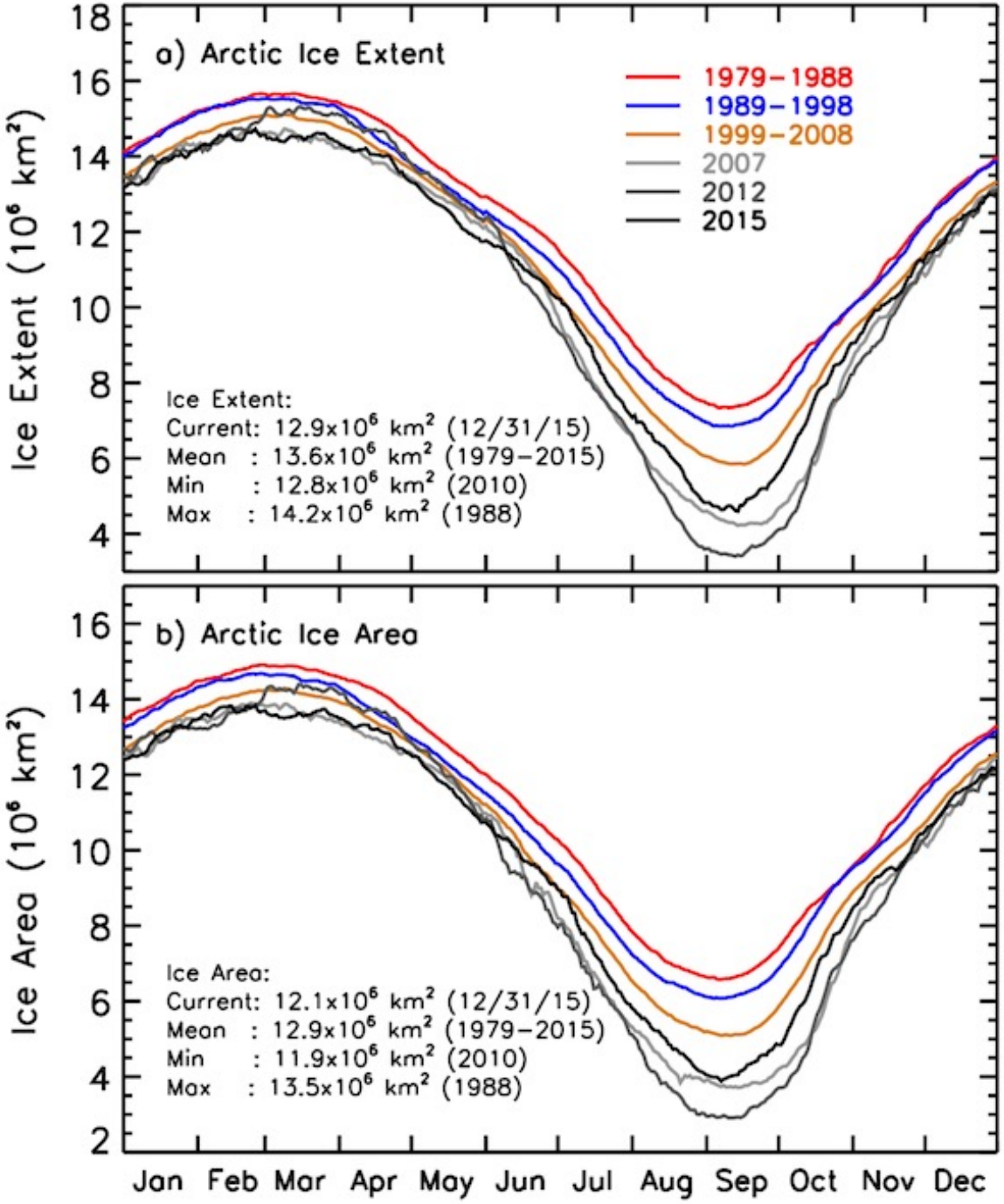
a) Arctic Ice Extent
1979–1988
1989–1998
1999–2008
2007
2012
2015
Ice Extent (10⁶ km²)
Ice Extent:
Current: 12.9x10⁶ km² (12/31/15)
Mean : 13.6x10⁶ km² (1979–2015)
Min : 12.8x10⁶ km² (2010)
Max : 14.2x10⁶ km² (1988)
b) Arctic Ice Area
Ice Area (10⁶ km²)
Ice Area:
Current: 12.1x10⁶ km² (12/31/15)
Mean : 12.9x10⁶ km² (1979–2015)
Min : 11.9x10⁶ km² (2010)
Max : 13.5x10⁶ km² (1988)
Jan Feb Mar Apr May Jun Jul Aug Sep Oct Nov Dec

September Arctic Sea Ice Extent

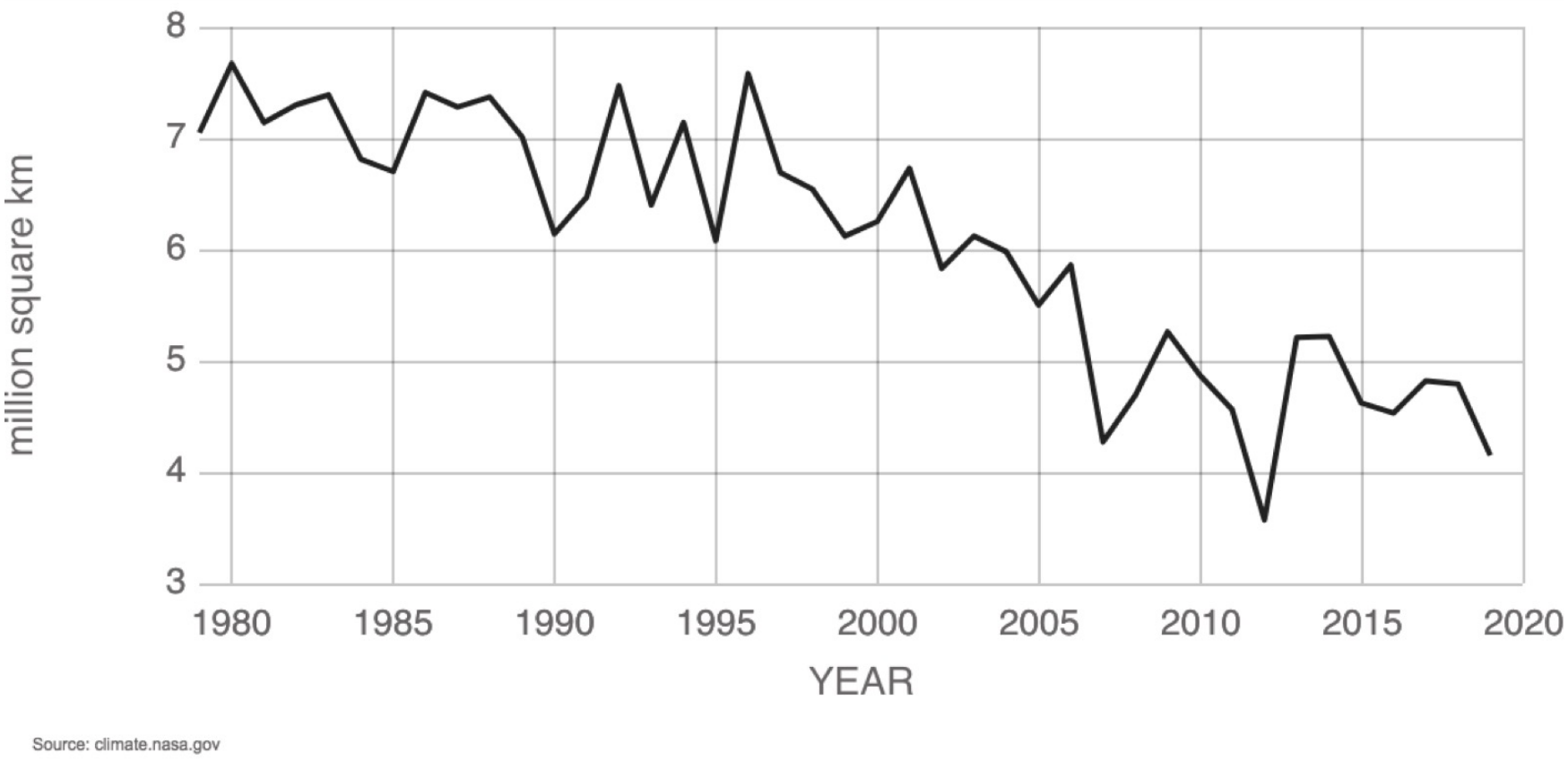

https://climate.nasa.gov/vital-signs/arctic-sea-ice/

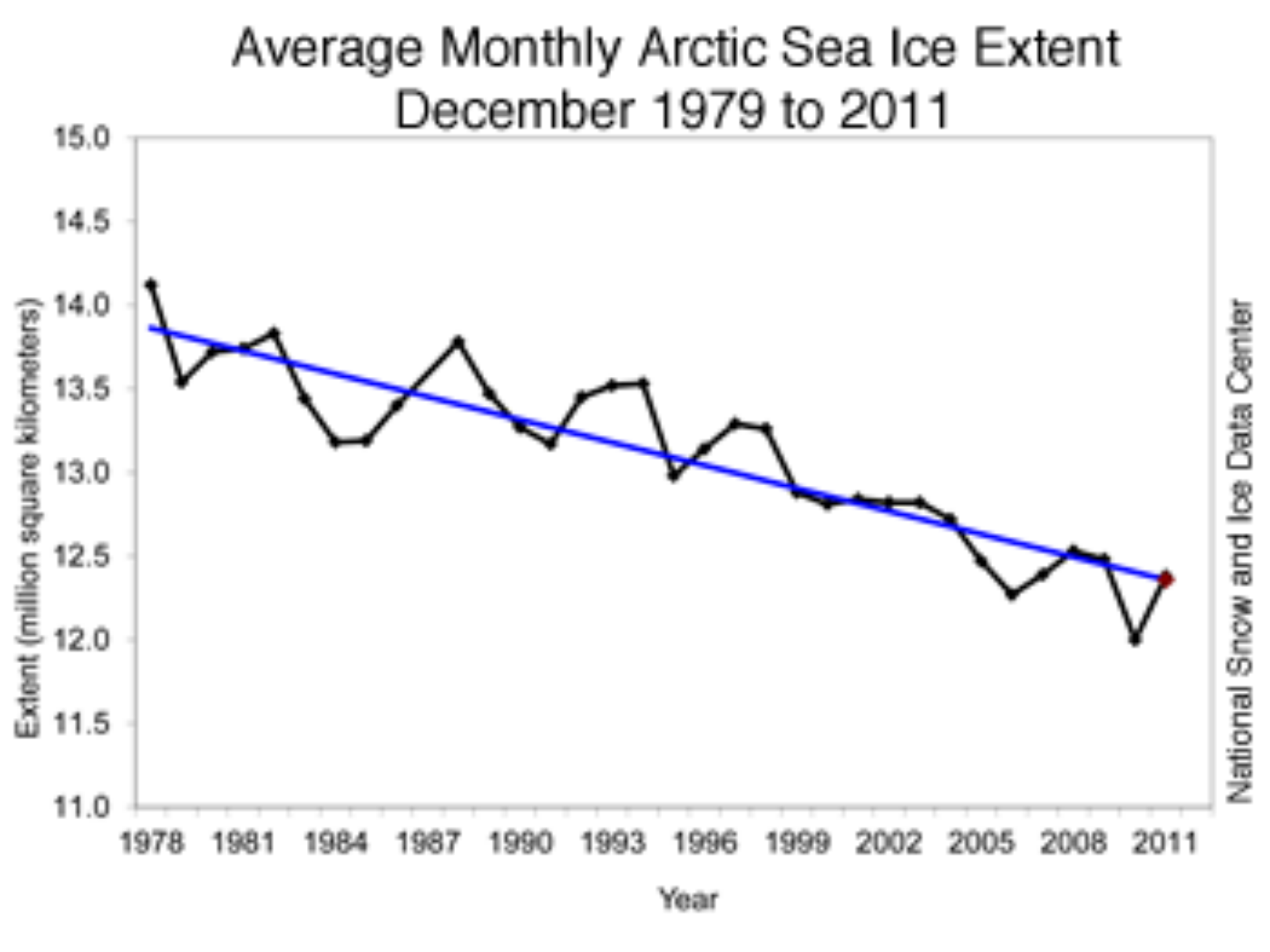
Average Monthly Arctic Sea Ice Extent
December 1979 to 2011
15.0
14.5
14.0
13.5
13.0
12.5
12.0
11.5
11.0
Extent (million square kilometers)
1978
1981
1984
1987
1990
1993
1996
1999
2002
2005
2008
2011
Year
National Snow and Ice Data Center

Northern Hemisphere, December 31, 2015

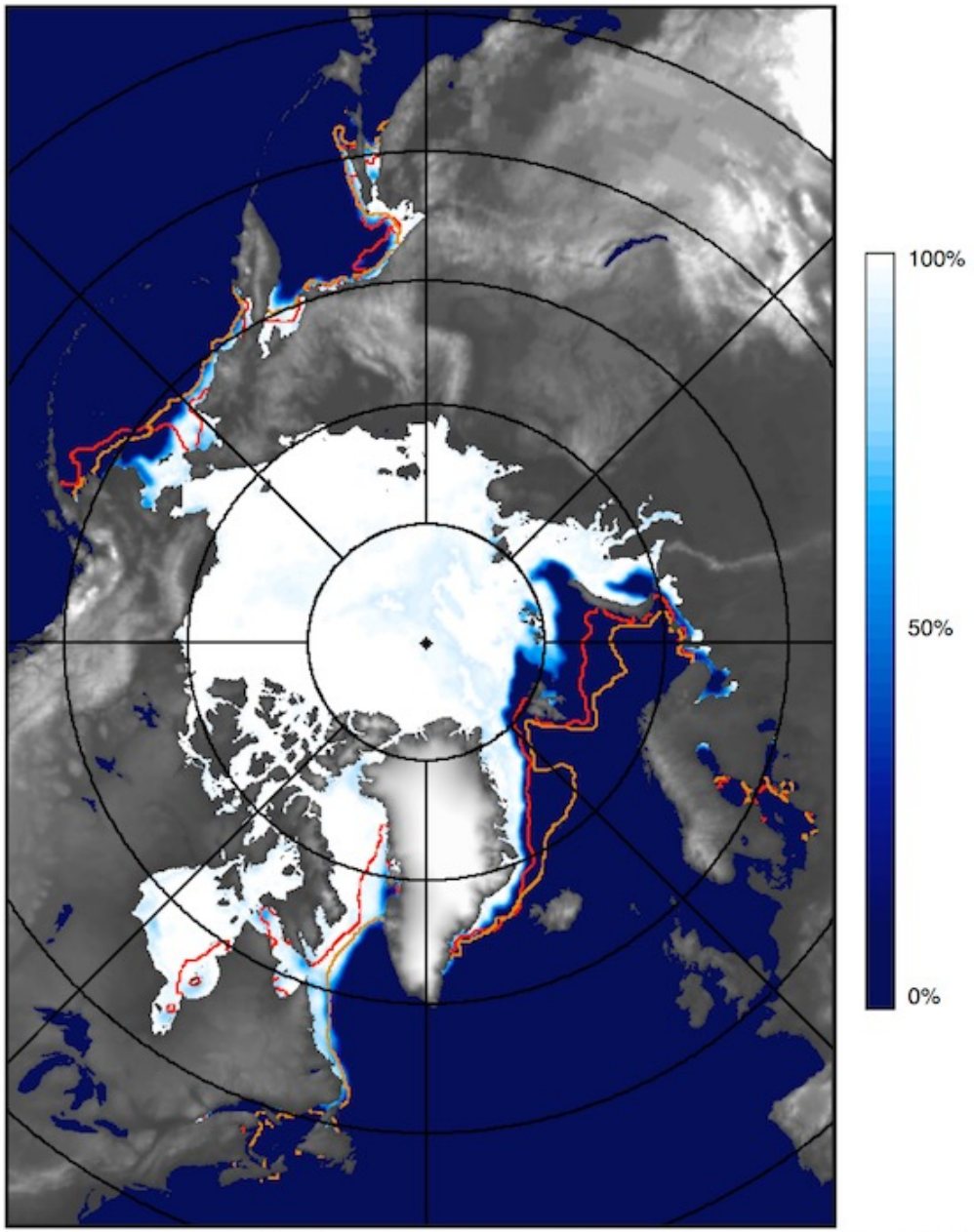

Current Ice Extent: $12.9 \cdot 10^6$ km^2

Minimum 12/31 Extent Outline, 2010 ($12.8 \cdot 10^6$ km^2)

Maximum 12/31 Extent Outline, 1988 ($14.2 \cdot 10^6$ km^2)

One Picture

Disappearing Act One of James Balog's most popular prints is this remarkable shot of a floating polar bear as seen above and below water. Photographed at the zoo in Portland, Oregon, with a battery of strobe lights placed at aquarium windows and on the ceiling, the bear "seems almost toylike and cuddly," Balog comments. "But you can sense its tremendous power." The picture, he adds, "also speaks to the global warming crisis and the knowledge that polar bears are losing their place on earth."

Facts: Insulated by two to six inches of fat against cold Arctic seas, polar bears can swim for hours without rest. Dog-paddling with their front paws and using their hind feet as rudders, they've been known to cross 100 to 150 miles of open water at a speed of 2 to 3 miles per hour. There are 19 subpopulations of polar bears scattered over the Arctic's vastness, and while the animals on Canada's western Hudson Bay, for one, have been well studied, other groups inhabit inaccessible areas. So scientists conjecture that the world's polar bear population might be 20,000 to 25,000 animals.

But polar bears depend on sea ice for their survival year-round, and summer sea ice is declining at a rate of about 8 percent per decade in the rapidly warming polar basin. Steven Amstrup, a wildlife biologist involved in an important new study on Alaska's Beaufort Sea that may produce bad news, puts it bluntly: "We know that the complete disappearance of sea ice would mean the end of polar bears."—*Les Line*

SPECIFICATIONS
Photographer: James Balog
Subject: Polar bear
Where: Oregon Zoo
Camera: Nikon F3 with 50mm lens
Film: Polaroid transparency


SULFUR

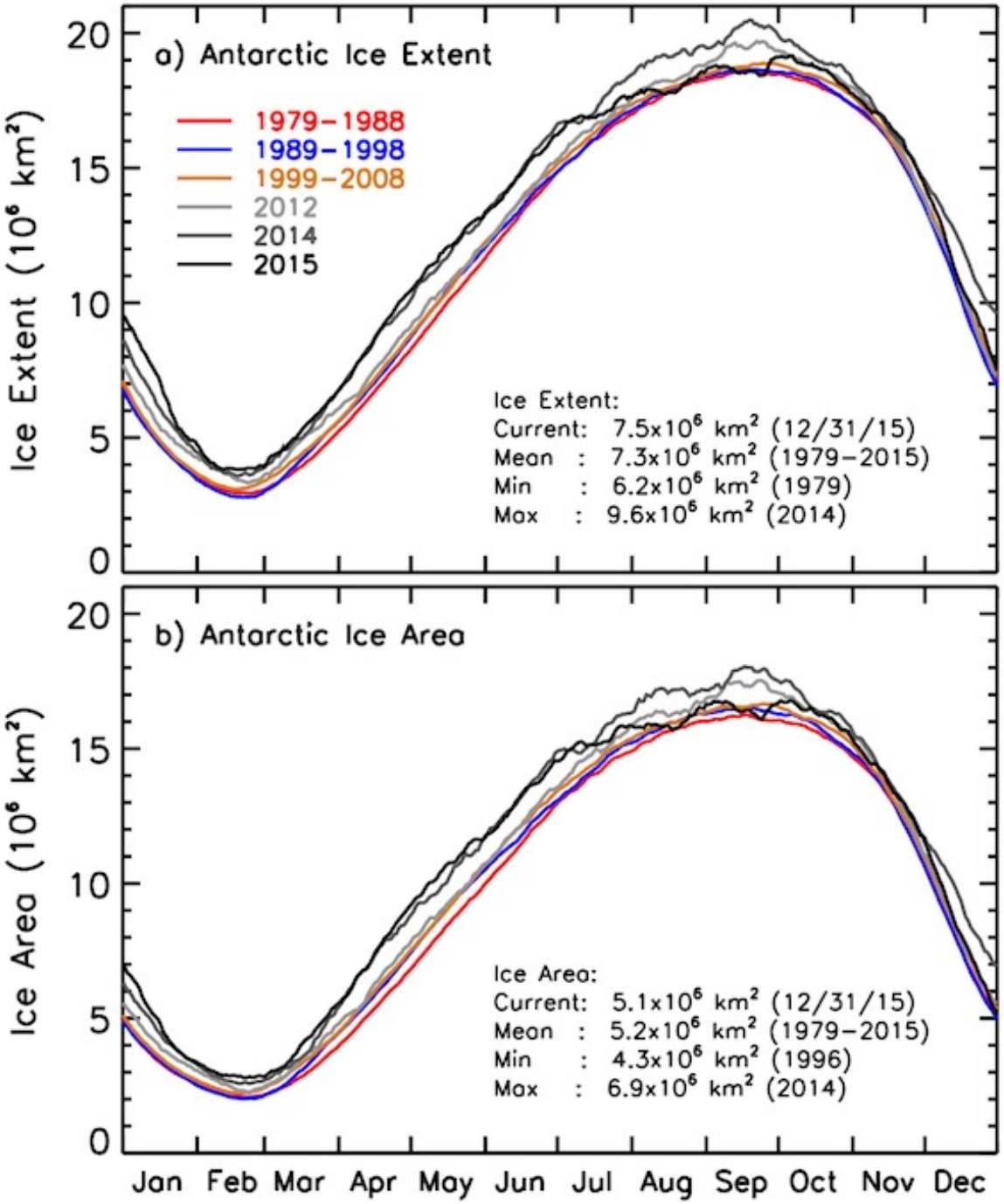
a) Antarctic Ice Extent
1979–1988
1989–1998
1999–2008
2012
2014
2015
Ice Extent (10⁶ km²)
Ice Extent:
Current: 7.5x10⁶ km² (12/31/15)
Mean : 7.3x10⁶ km² (1979–2015)
Min : 6.2x10⁶ km² (1979)
Max : 9.6x10⁵ km² (2014)
b) Antarctic Ice Area
Ice Area (10⁶ km²)
Ice Area:
Current: 5.1x10⁶ km² (12/31/15)
Mean : 5.2x10⁶ km² (1979–2015)
Min : 4.3x10⁶ km² (1996)
Max : 6.9x10⁵ km² (2014)
0
5
10
15
20
Jan Feb Mar Apr May Jun Jul Aug Sep Oct Nov Dec

Southern Hemisphere, December 31, 2015

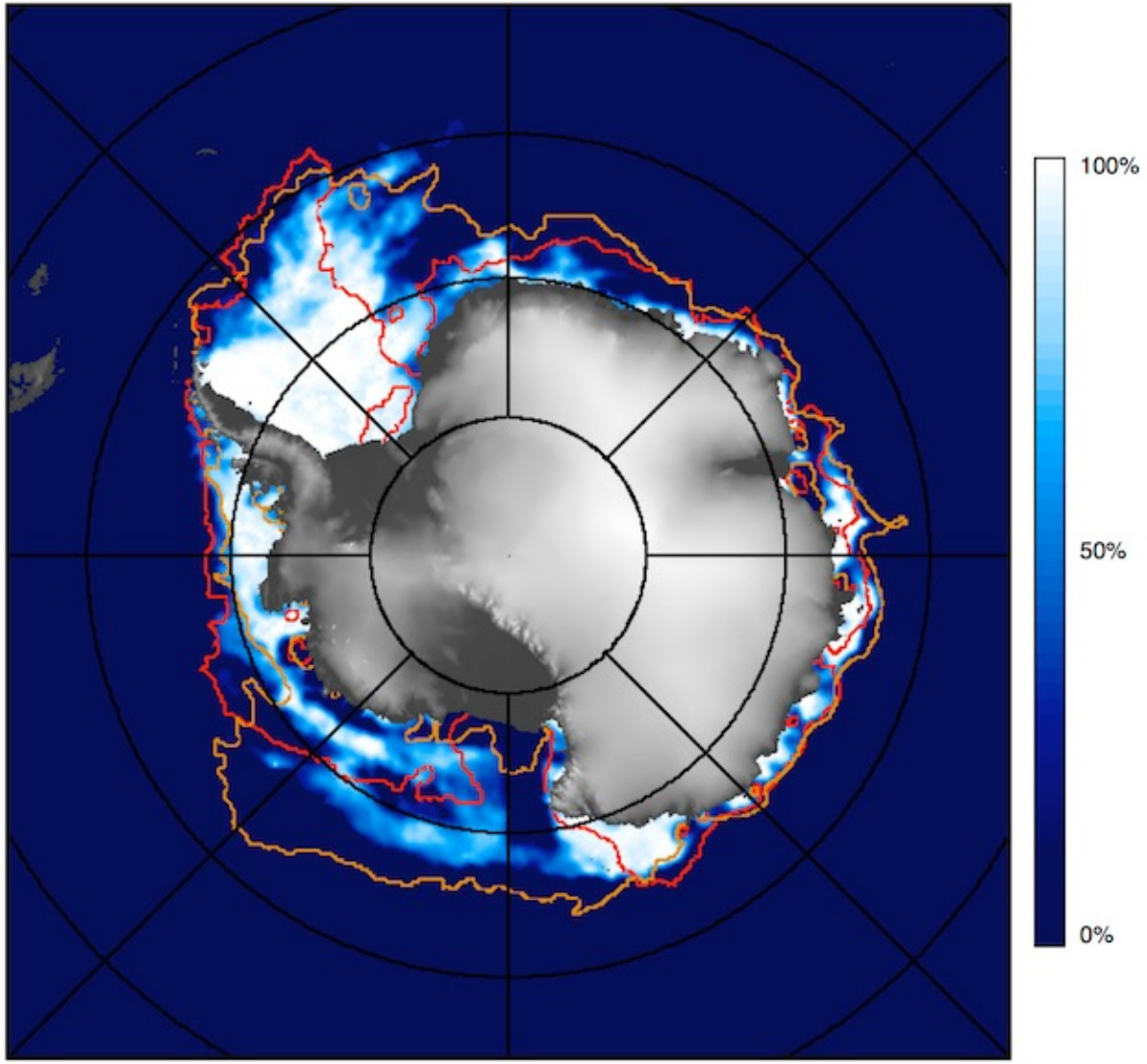

Current Ice Extent: $7.5 \cdot 10^6$ km^2

Minimum 12/31 Extent Outline, 1979 ($6.2 \cdot 10^6$ km^2)

Maximum 12/31 Extent Outline, 2014 ($9.6 \cdot 10^6$ km^2)

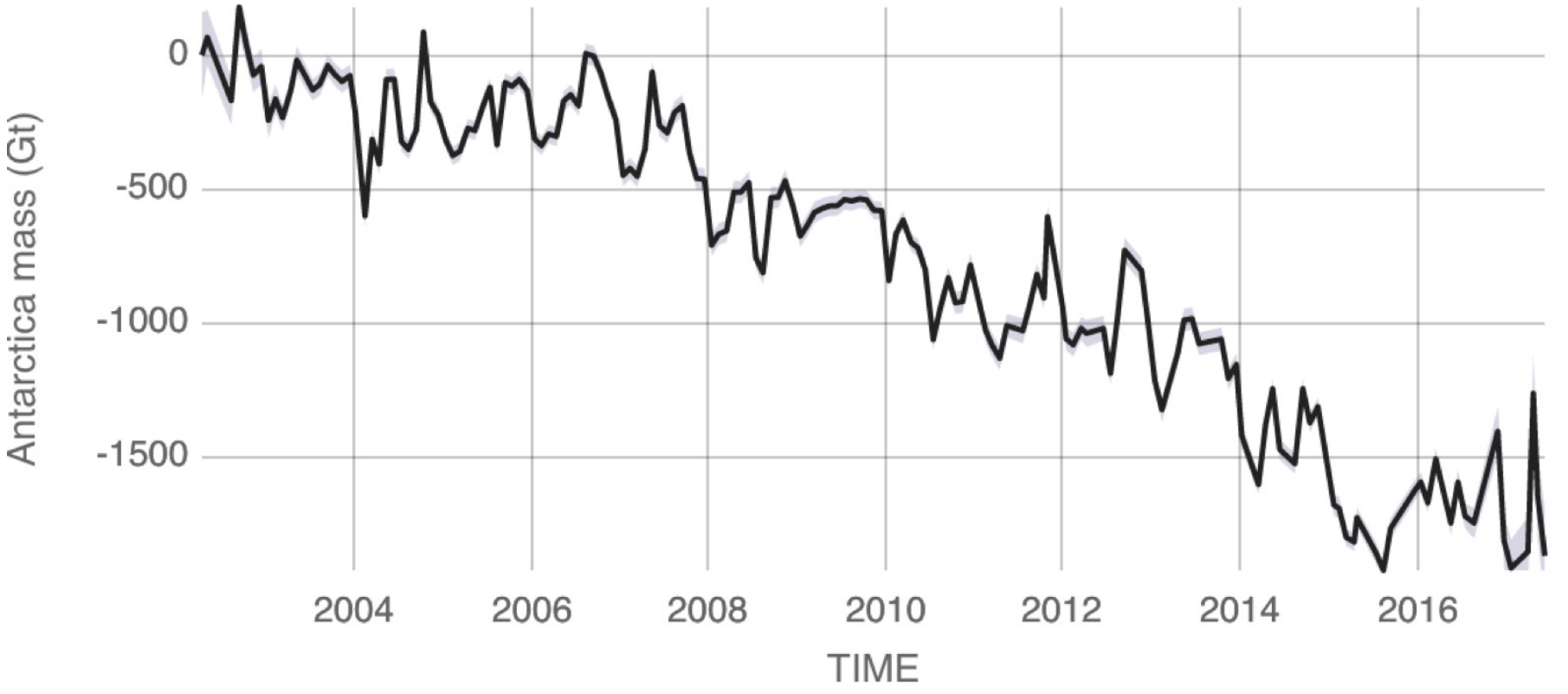

Source: climate.nasa.gov

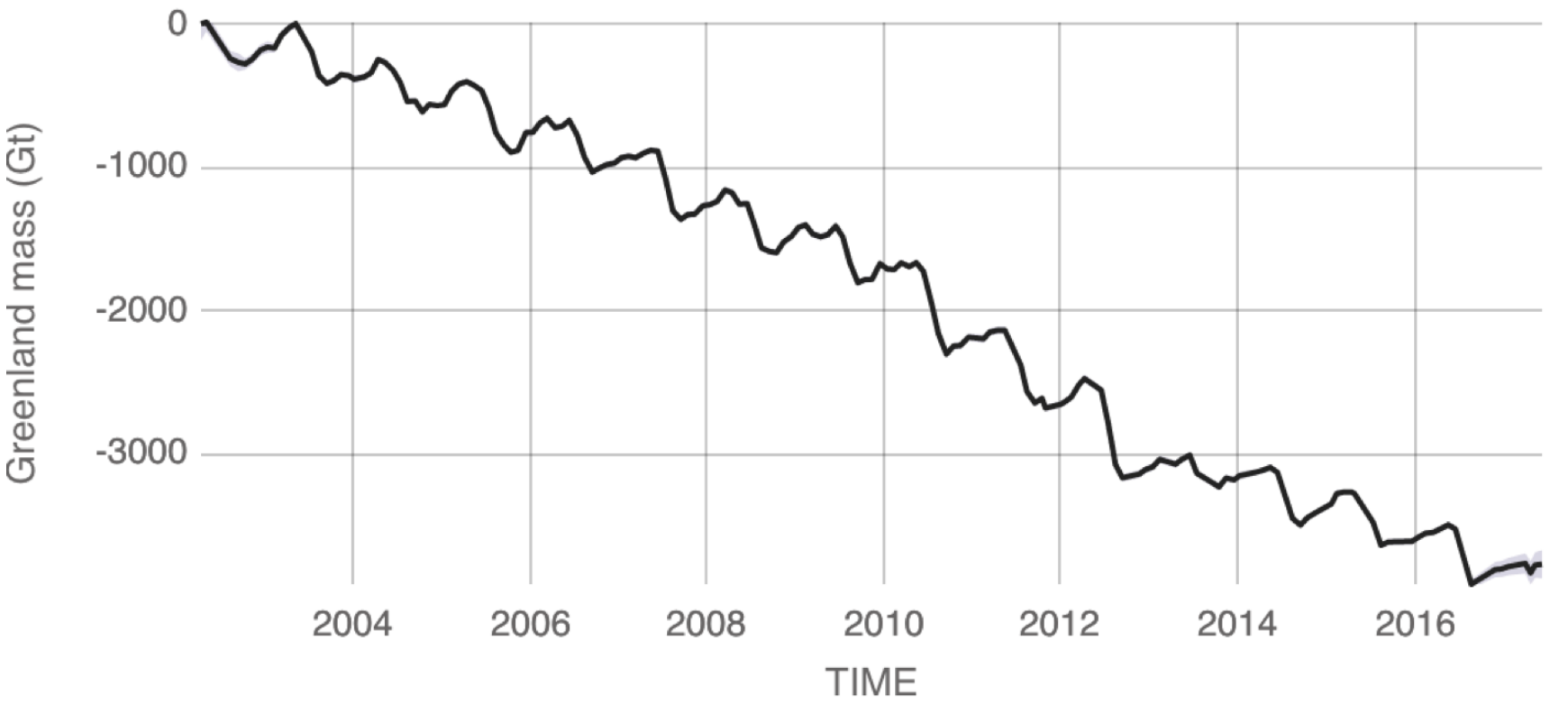

Source: climate.nasa.gov

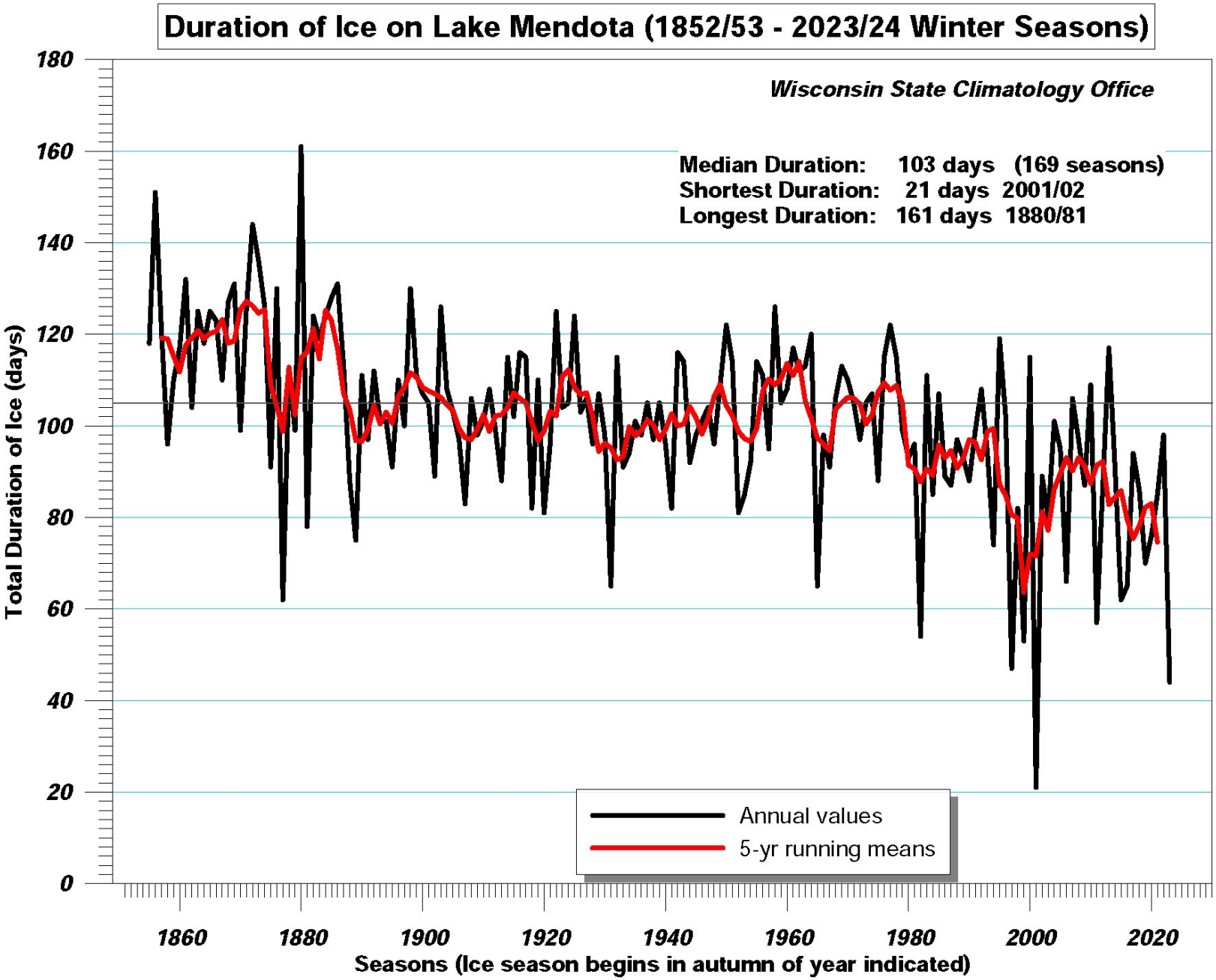
Duration of Ice on Lake Mendota (1852/53 - 2023/24 Winter Seasons)
Wisconsin State Climatology Office
Median Duration: 103 days (169 seasons)
Shortest Duration: 21 days 2001/02
Longest Duration: 161 days 1880/81
Total Duration of Ice (days)
180
160
140
120
100
80
60
40
20
0
1860
1880
1900
1920
1940
1960
1980
2000
2020
Seasons (Ice season begins in autumn of year indicated)
Annual values
5-yr running means

Summer Sea Surface Temperatures by Ocean Basin 1970-2005

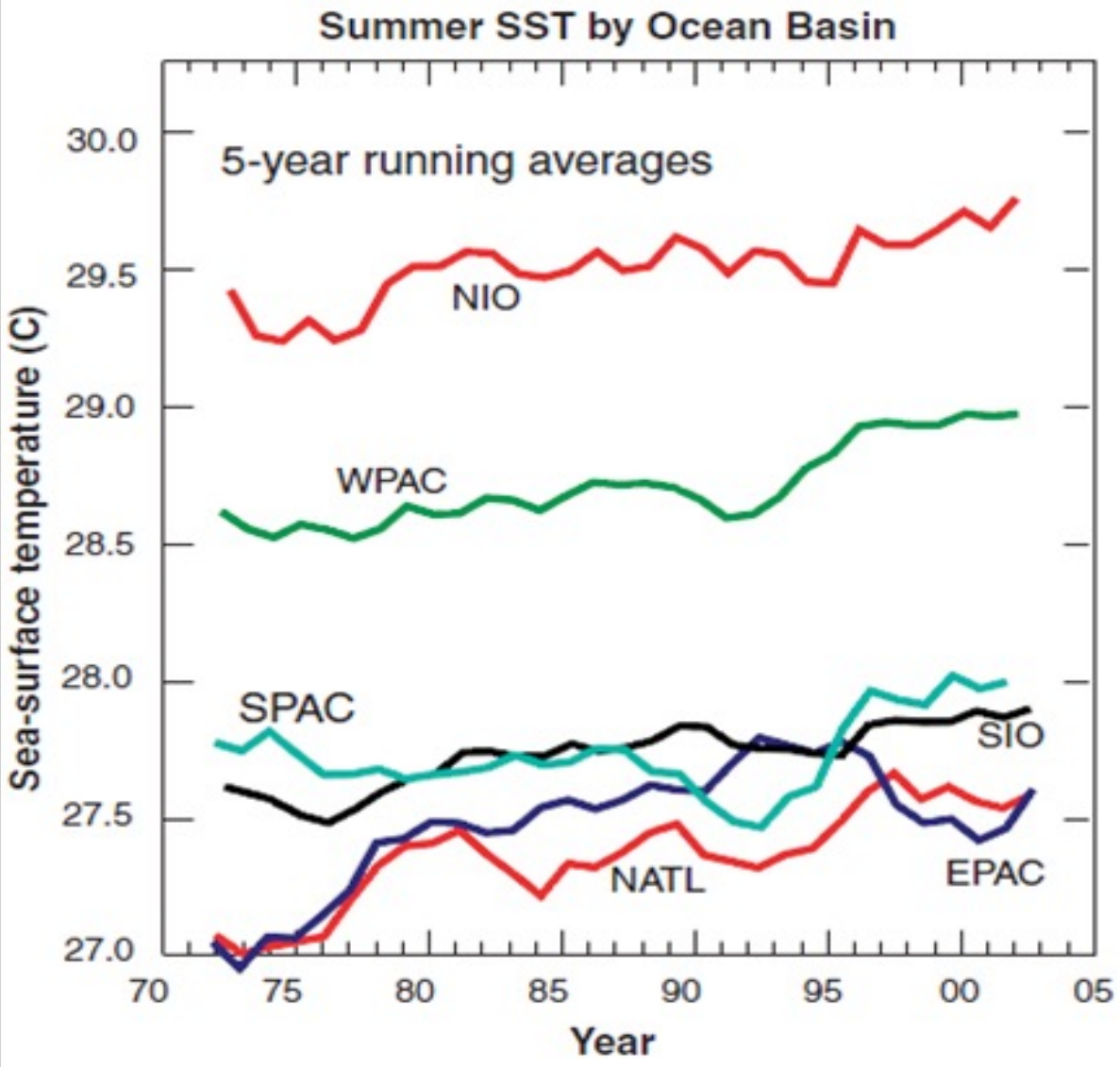

Fig. 1. Running 5-year mean of SST during the respective hurricane seasons for the principal ocean basins in which hurricanes occur: the North Atlantic Ocean (NATL: 90° to 20°E, 5° to 25°N, June-October), the Western Pacific Ocean (WPAC: 120° to 180°E, 5° to 20°N, May-December), the East Pacific Ocean (EPAC: 90° to 120°W, 5° to 20°N, June-October), the Southwest Pacific Ocean (SPAC: 155° to 180°E, 5° to 20°S, December-April), the North Indian Ocean (NIO: 55° to 90°E, 5° to 20°N, April-May and September-November), and the South Indian Ocean (SIO: 50° to 115°E, 5° to 20°S, November-April).

Global Tropical Cyclones 1970-2005

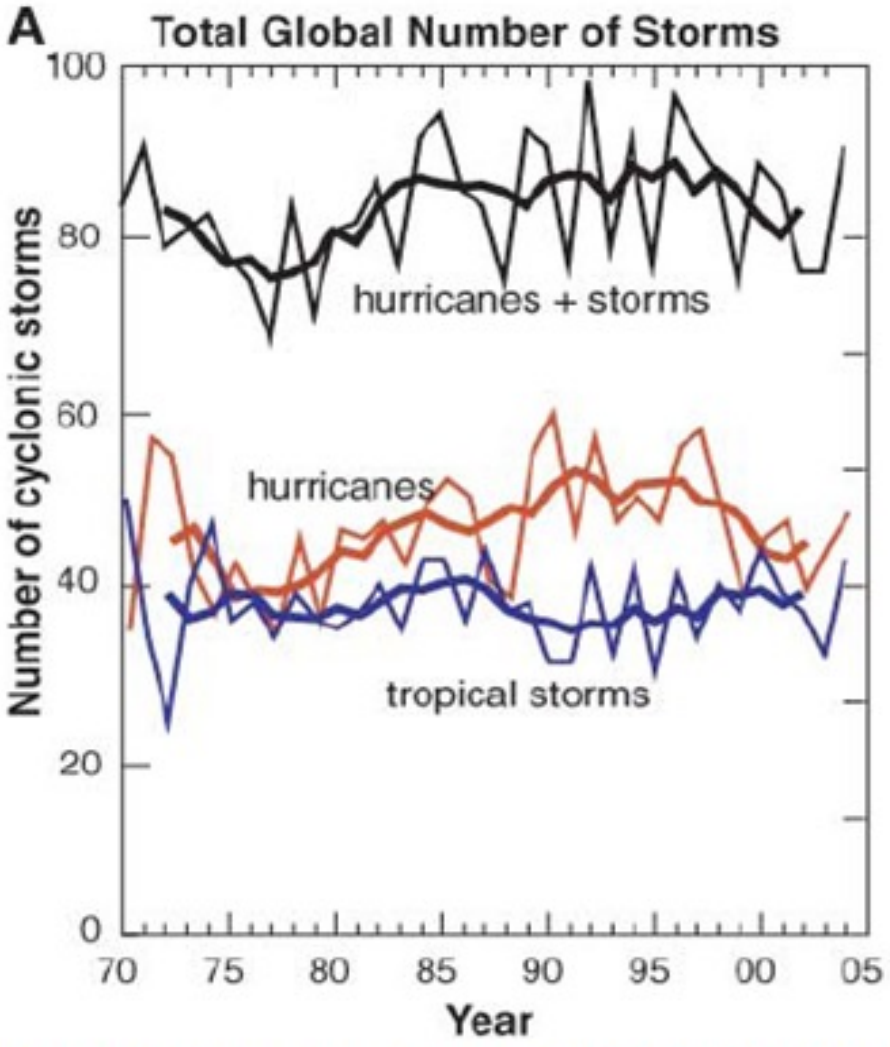

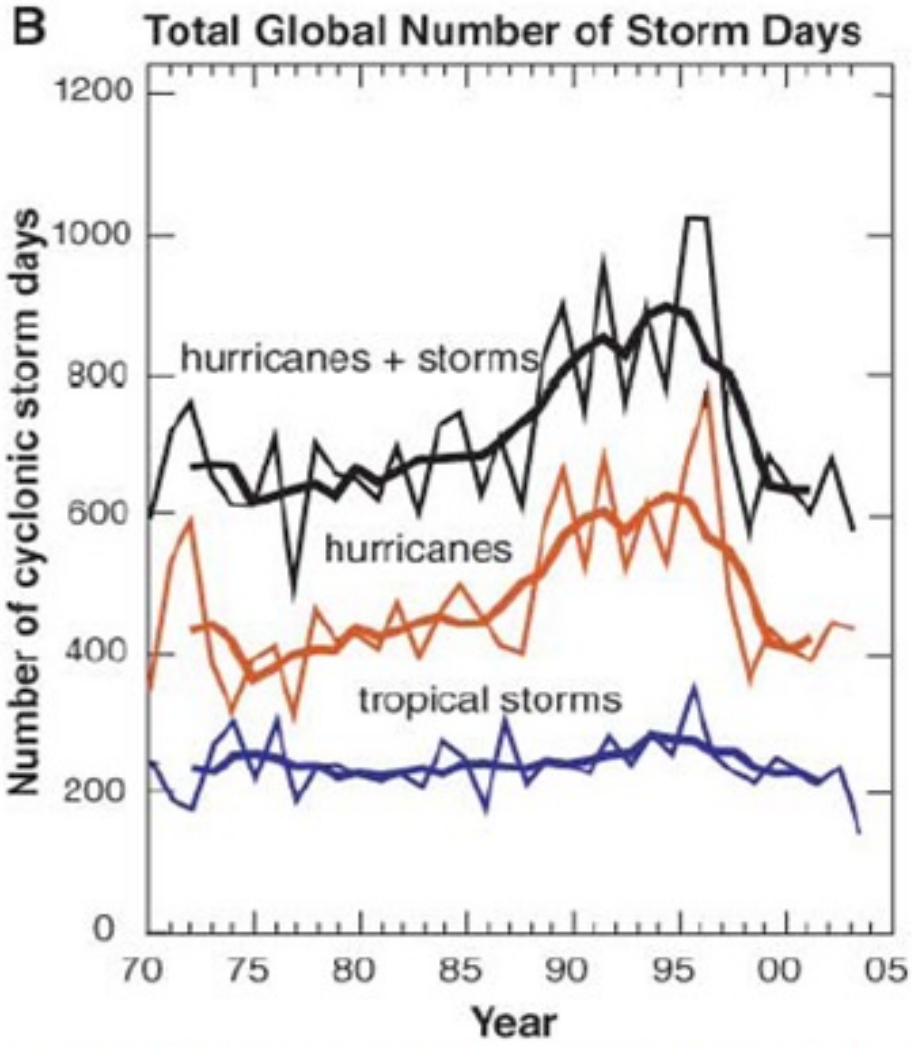

Fig. 2. Global time series for 1970–2004 of (A) number of storms and (B) number of storm days for tropical cyclones (hurricanes plus tropical storms; black curves), hurricanes (red curves), and tropical storms (blue curves). Contours indicate the year-by-year variability, and the bold curves show the 5-year running average.

Atlantic Tropical Cyclones 1880-2008

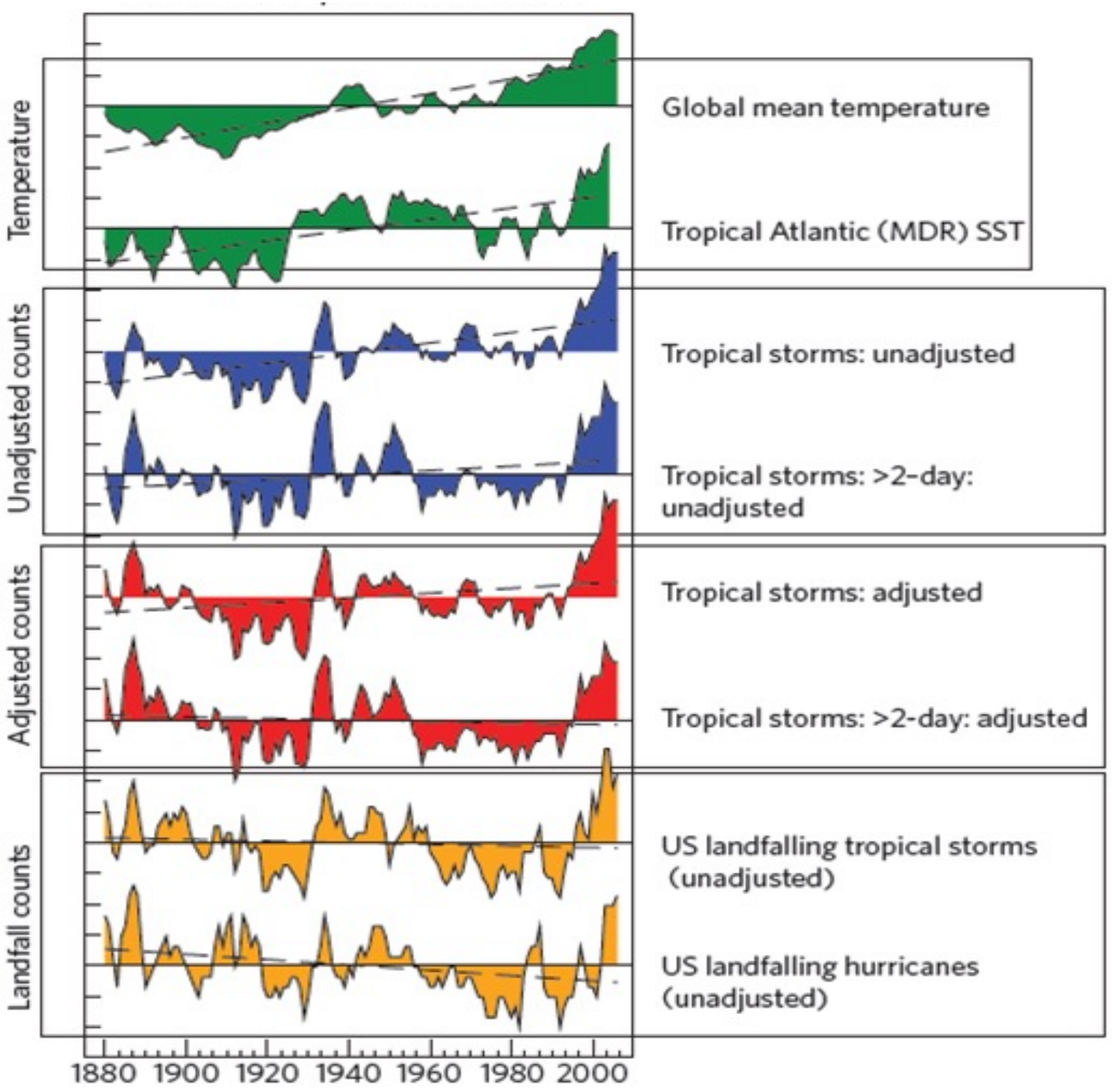

Major Atlantic Hurricanes 1944 - 2000

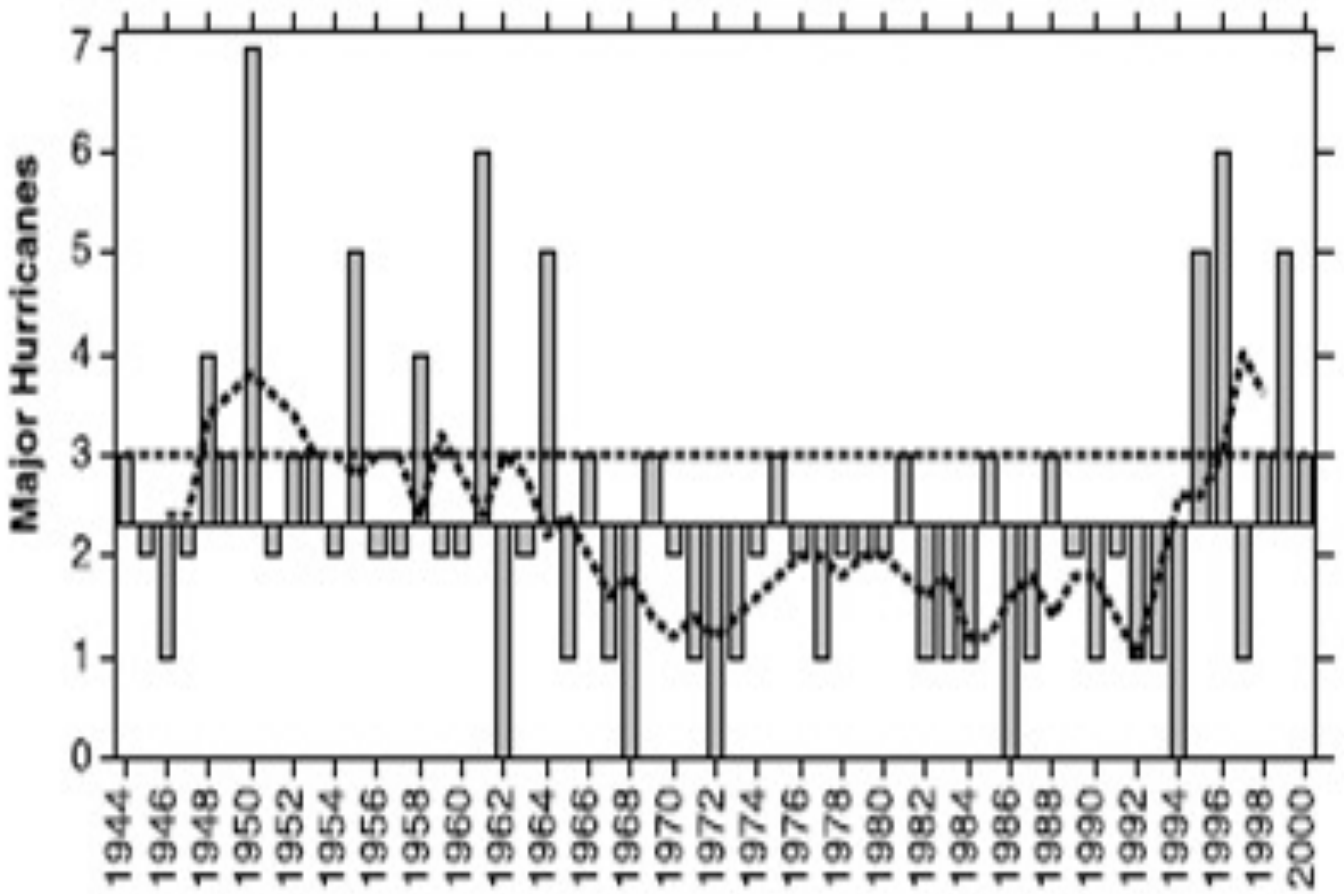

Fig. 1. Number of major hurricanes from 1944 through 2000 (*32*). Less reliable data before routine aircraft reconnaissance dictate caution in the use of these data before 1944 (*33*). Solid horizontal reference line corresponds to sample mean (2.3). Dashed curved line is 5-year running mean. Also shown is the threshold of three major hurricanes per year (dashed straight line).

Tropical Atlantic SON Area with Weak Vertical Wind Shear 1944 - 2000

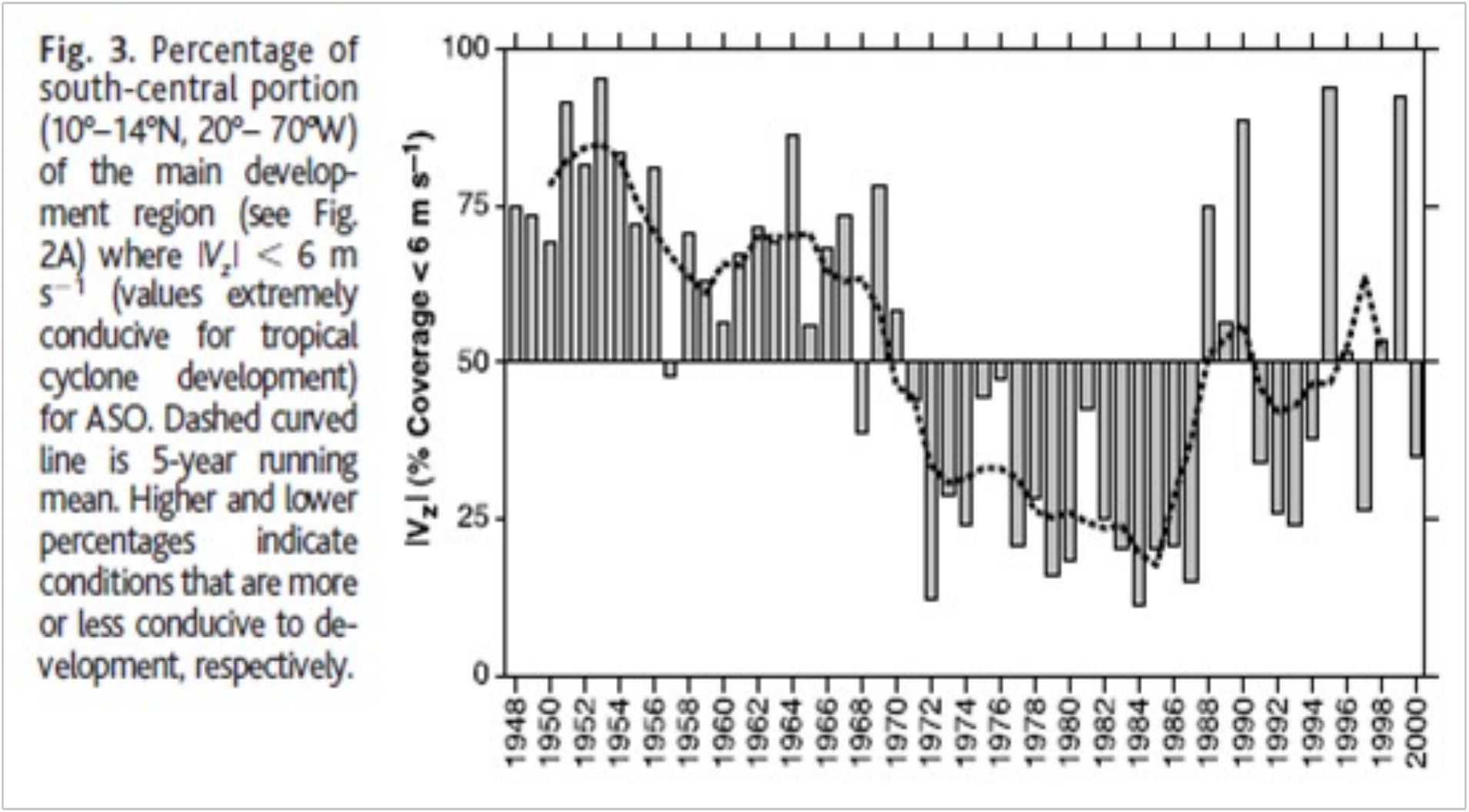

Fig. 3. Percentage of south-central portion (10°–14°N, 20°–70°W) of the main development region (see Fig. 2A) where $|V_z| < 6$ m s^{-1} (values extremely conducive for tropical cyclone development) for ASO. Dashed curved line is 5-year running mean. Higher and lower percentages indicate conditions that are more or less conducive to development, respectively.

Atlantic Meridional Mode Variation 1870 - 2000

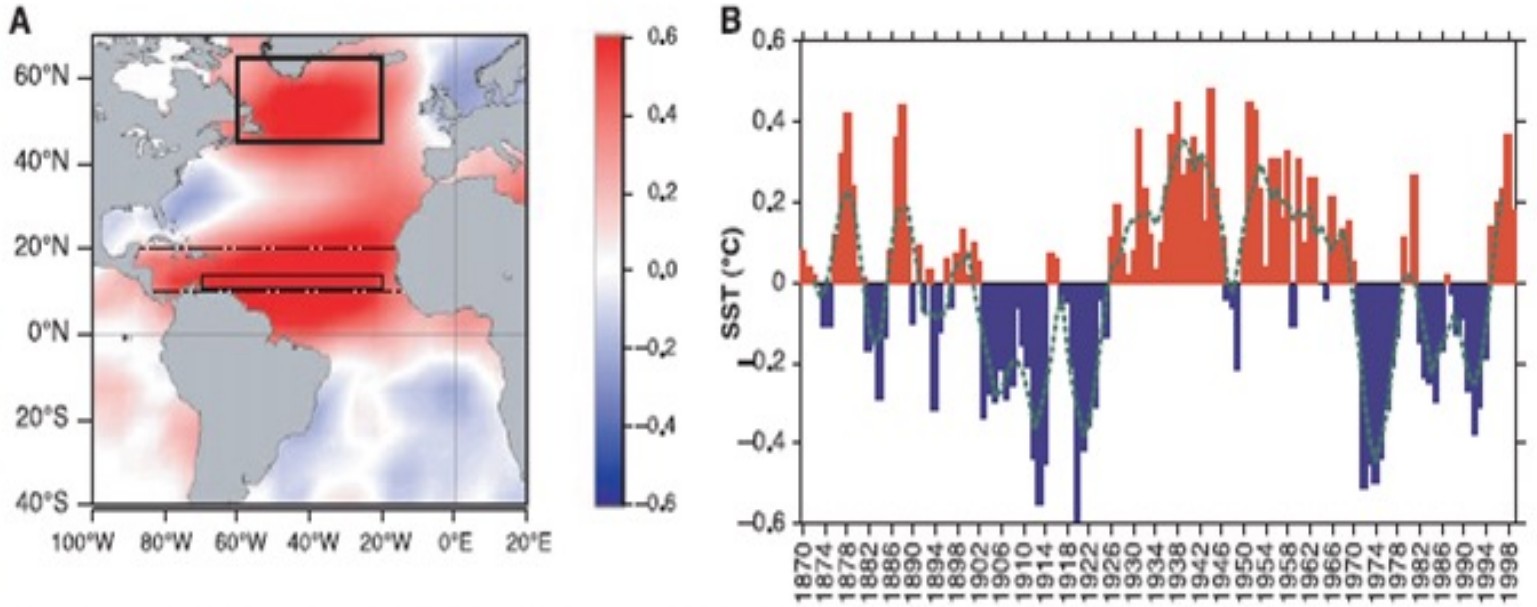

Fig. 2. Atlantic sector of the first rotated EOF of non-ENSO global SST variability for 1870–2000 referred to as the "Atlantic multidecadal mode" (*38*, *39*). (**A**) Spatial distribution of correlations between local monthly SST anomalies and the modal reconstruction over the indexed region (northern rectangle), the general area where the mode amplitude is the strongest. This distribution has a similar spatial structure to the actual rotated EOF and gives a measure of the local fractional variance (squared temporal correlation) accounted for at each grid point. Dashed lines give north and south boundaries of main development region (MDR) and box (10° to 14°N, 20° to 70°W) is region used to calculate data for Fig. 3. (**B**) Temporal reconstruction (annual means) of the mode-related variability averaged over the rectangular areain (A). Dashed curved lineis 5-year running mean. Although the signal is stronger in the North Atlantic, it is global in scope with positively correlated co-oscillations in parts of the North Pacific (*55*). For the multidecadal variations shown here, the coherence between the MDR and far North Atlantic is a robust feature. The SST fluctuations in the far North Atlantic could be used as a proxy for changes in the MDR.

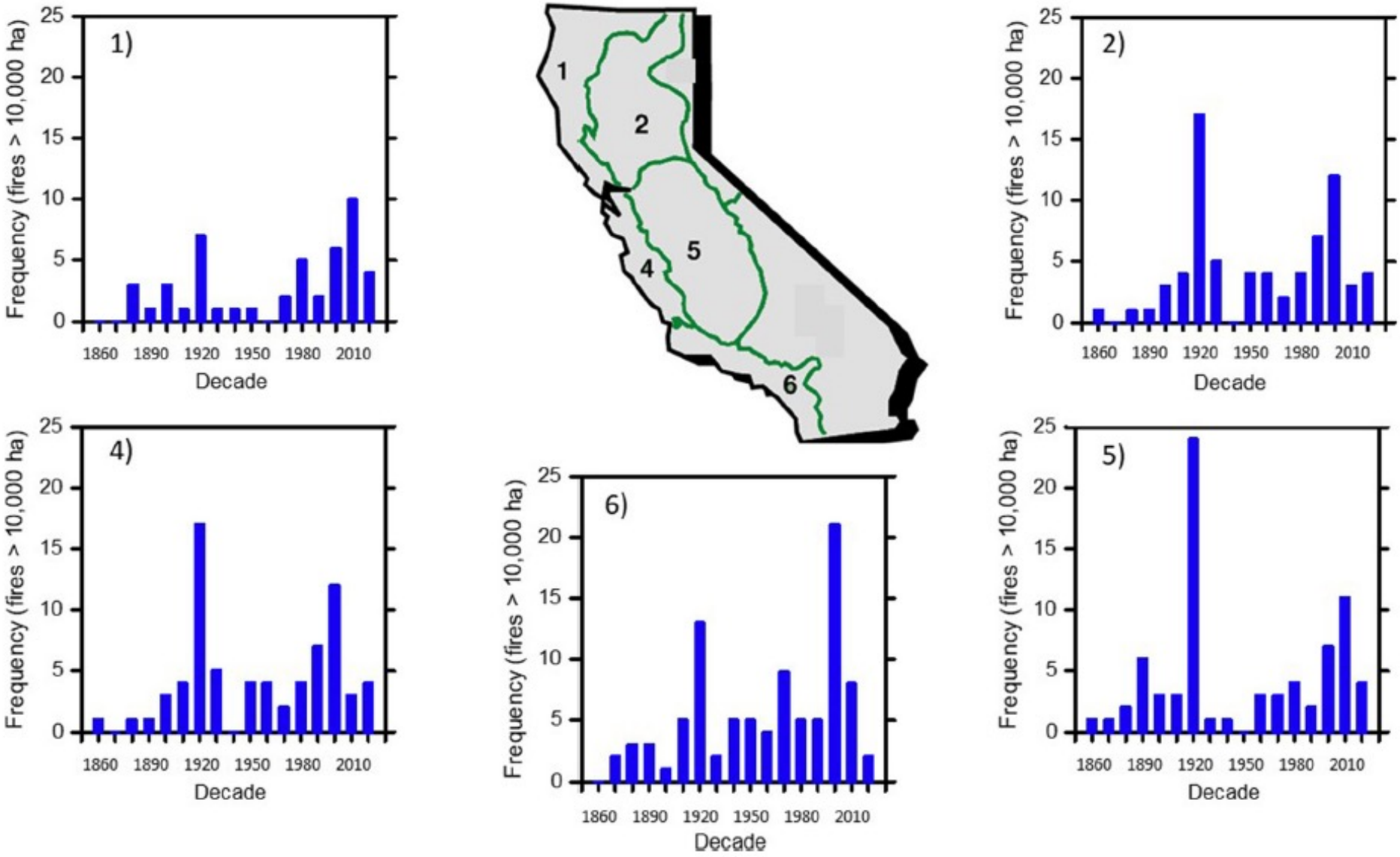

Fig. 3 Decadal frequency of large fires within NOAA Divisions. Note the decade 2020 is represented by a single year.

Keely and Syphard, Fire Ecology, 2021